ALMA MATER STUDIORUM
UNIVERSITÀ DI BOLOGNA

DOTTORATO DI RICERCA IN

Biologia Cellulare e Molecolare

Ciclo XXXVI

Settore Concorsuale: 05/E2

Settore Scientifico Disciplinare: BIO/11

TARGETING THE ESSENTIAL TRANSCRIPTIONAL REGULATOR HP1043 FOR NOVEL ANTIMICROBIAL APPROACHES IN *HELICOBACTER PYLORI* INFECTION

Presentata da: ***Federico Antoniciello***

Coordinatore Dottorato

Prof. Vincenzo Scarlato

Supervisore

Prof. Vincenzo Scarlato

Co-supervisore

Prof. Davide Roncarati

Esame finale anno 2024

CONTENTS

SHORT CV

PUBLICATIONS

Antoniciello F., Nejad A.J., Chiti E., Roncarati D., Scarlato V., Nielsen P.E. "Antisense Peptide Nucleic Acid Targeting the *Helicobacter pylori* Essential Transcriptional Regulator HP1043". *In preparation*

Fiore C., **Antoniciello F.**, Roncarati D., Scarlato V., Braga D. "Levofloxacin and ciprofloxacin co-crystals with flavonoids: solid-state investigation for a multi-target strategy against *Helicobacter pylori*". *Submitted*

Vannini A., Roncarati D., D'Agostino F., **Antoniciello F.**, Scarlato V. "Insights into the Orchestration of Gene Transcription Regulators in *Helicobacter pylori*", Int. J. Mol. Sci. 2022, 23, 13688, doi: 10.3390/ijms232213688.

Antoniciello F., Roncarati D., Zannoni A., Chiti E., Scarlato V. and Chiappori F. "Targeting the Essential Transcriptional Factor HP1043 of *Helicobacter pylori*: A Drug Repositioning Study", Front. Mol. Biosci., 9:887564, doi: 10.3389/fmolb.2022.887564

CONGRESSES

Antoniciello F., Chiti E., Zannoni A., Nejad A.J., Nielsen P.E., Roncarati D., Scarlato V. "Targeting *Helicobacter pylori* Transcriptional Regulator HP1043 as a Novel Antimicrobial Approach". SIMGBM XXXIV Congress 2023, Cagliari, 21-23 September 2023 - Poster.

Antoniciello F., Zannoni A., Roncarati R., Scarlato V., and Nielsen P.E. "Does Helicobacter pylori Have a Switch?". Molecular Microbiology Conference, Birmingham, September 15-16, 2022 - Oral presentation

Antoniciello F., Zannoni A., Chiti E., Roncarati D., Scarlato V. "Inhibition of the essential transcriptional regulator HP1043 as a potential therapeutic approach against *Helicobacter pylori* infection". Cortona Procarioti 2022 SIMGBM, Cortona, 23-25 June 2022.

RESEARCH FELLOWSHIP

Visiting Ph.D. student at the "Center for Peptide-Based Antibiotics", Department of Cellular and Molecular Medicine, University of Copenhagen, (3 months) 2022-23, funded by FEMS Research and Training Grant (RTG).

COURSES

Scientific Artwork for Publication and Presentation. Lecturer: *Prof*. Alberto Danielli.

Biocrystallography. Lecturer: *Dr*. Luca Mazzei.

Handling of Radioisotopes in Biology. Lecturer: *Prof*. Alberto Danielli.

Basic course in Science of Laboratory Animals. Organizers: *Dr*. Valentina Vasina, Prof. Barbara Monti.

Annual workshop on the topics of Research in Molecular and Cellular Biology. Organizers: *Prof*. Vincenzo Scarlato / *Prof*. Davide Roncarati.

TUTORING ACTIVITIES

Year 2021/22: **Laboratory of molecular biology** (30 h) for the master's degree course in Chemistry and Pharmaceutical Technologies. Lecturer: *Prof*. Alberto Leoni.

Year 2021/22: **Laboratory of molecular biology** (27 h) for the bachelor's degree course in Genomics. Lecturer: *Prof*. Francesco Musiani.

ABSTRACT

Helicobacter pylori is a highly prevalent and pathogenic bacterium that colonises the gastric mucosa and is responsible for various gastrointestinal disorders such as chronic gastritis, peptic ulcers and gastric cancer. Remarkably, the bacterium exhibits rapid development of resistance to standard antibiotics, reducing the effectiveness of therapies and eradication efforts, and posing a growing threat to public health. The growing challenge of antimicrobial resistance calls for new strategies. Innovative approaches are exploring the potential of targeting bacterial transcriptional regulators (TRs) modulating the expression of essential genes. Among the TRs in *H. pylori*, HP1043 was discovered as a crucial factor that has control over several cellular processes. As this regulator plays a central role, its gene cannot be deleted, and the protein's level cannot be modulated to study its regulatory role. This intrinsic property renders it a challenging research subject yet places it as a potential focus for innovative antimicrobial strategies. In this study, we employed a gene reporter system to investigate HP1043's regulatory function *in vivo* and *in vitro* on a cluster of validated targets. This approach allows us also to study the effect of a variable distance between the HP1043 consensus sequence and the -10 Pribnow box element on its transcription regulation. In parallel, *in silico* screening and drug repositioning methods involving high-throughput-virtual-screening and molecular dynamics simulations were employed to identify candidate compounds that could inhibit HP1043's DNA-binding activity. Secondly, a crystal engineering approach aiming to reduce antibiotic dosage was employed to generate co-crystals capable of exploiting multiple mechanisms of action including the reported inhibitory activity on HP1043 binding. Finally, we explored the potential and versatility of peptide nucleic acids (PNAs) in modulating HP1043 expression. As short antisense oligomers, PNAs demonstrated to selectively block the translation of target genes, leveraging their precise gene knockdown capacity for antimicrobial purposes. This work represents the first examples of multi-targeting antimicrobial strategies against *H. pylori*, with a focus on the crucial regulator HP1043 and its regulatory mechanisms.

1. INTRODUCTION

1.1. Helicobacter pylori: epidemiology and treatments

Helicobacter pylori is a gram-negative, microaerophilic, spiral-shaped bacterial pathogen, and is one of the most successful human pathogens, affecting roughly half of the global population[1]. Initially isolated in 1982 by Robin Warren and Barry Marshall, the bacterium has been identified as the main cause of various severe gastrointestinal disorders, such as chronic active gastritis, peptic ulcers, mucosa-associated lymphoid tissue (MALT) lymphoma, and gastric adenocarcinoma[2,3]. Whilst chronic gastritis is the primary result of *H. pylori* carriers, only 1% of them will develop correlated gastric malignancies. However, given the pathogenicity data and the public health concern, the World Health Organization (WHO) has not only classified *H. pylori* as a group I carcinogen but also included it in its list of antibiotic-resistant pathogens of significant threat to human health in 2017[4]. The bacterium length of approximately 3.0 to 4.0 μm and its unique morphology are considered to be an adaptation that facilitates its colonization and persistence in the stomach[5]. Moreover, *H. pylori* possesses a flagellar apparatus that confers its vital motility, allowing it to navigate through the viscous environment of the gastric mucosa, and penetrate the mucus layer, where specialized adhesins facilitate its attachment to the gastric epithelial cells[6]. The bacterium's successful colonization of the human gastric mucosa, a particularly inhospitable niche, is mediated by a repertoire of well-regulated virulence factors. Urease activity plays a critical role in initial colonization by neutralizing the stomach's acidic environment, facilitating further bacterial invasion[7]. Furthermore, *H. pylori* possesses the capacity to evade the immune responses of the host, whether innate or adaptive. This is achieved by reducing the antigenicity of its pathogen-associated molecular patterns, which enables it to elude detection by the host's innate immune system. It also carries out immunomodulatory actions that weaken the host's adaptive immune responses, thus facilitating its long-term persistence. Despite the immune evasion strategies of *H. pylori*, the infection triggers a robust immune response that is frequently non-protective and even

contributes to the pathogenesis[8,9]. *H. pylori* employs an array of virulence factors such as the vacuolating toxin (VacA), which is secreted forms pores, and the cag pathogenicity island (CagA), which is transferred to host cells by the cag-type IV secretion system, that collaborate to cause cellular damage and trigger pro-inflammatory cytokines production, ultimately leading to the development of the disease. The reasons behind the bacterium's production of these factors are not fully understood, but several studies suggested that they may be linked to persistent strategies such as increased nutrient absorption or greater diffusion within the gastric mucosa[7,10]. Conventional therapeutic treatments for *H. pylori* infections traditionally involve a combination of proton pump inhibitors (PPI) and antibiotics, such as clarithromycin, amoxicillin, and metronidazole, or bismuth subcitrate, metronidazole and tetracycline[11,12]. However, the emergence of antibiotic-resistant strains has compromised treatment efficacy, with eradication cure rates often falling below 70%, necessitating a shift toward quadruple antibiotic therapy regimens[13]. If conventional methods are unsuccessful, it may be necessary to conduct antimicrobial susceptibility testing[11,14]. Although, the bacterium's fastidious nature can make such phenotypic techniques problematic, requiring molecular approaches to determine antibiotic resistance. Due to the bacterium's rapid increase in antibiotic resistance, there is a pressing requirement for novel therapeutic strategies. Vaccine development has been hindered by various factors, such as the absence of identifiable antigens and the frequently non-protective immune reaction caused by chronic *H. pylori* infections[15]. Hence, it is crucial to identify new and specific targets to develop new therapeutic approaches to tackle this global health issue.

1.2. Genomic landscape and regulatory functions

In the intricate realm of microbial genomics, *H. pylori* emerges as a remarkable example of adaptation and specialisation within the bacterial world. With its spiral shape and microaerophilic nature, this bacterium has successfully found a niche in the human gastric environment, adapting its genome and regulatory machinery to

thrive in this particular habitat. Studies elucidating *H. pylori* genomic architecture and the intricacies of its regulatory functions provide fascinating insights into the evolutionary pathogenicity strategies[16,17]. At the core of *H. pylori*'s genomic identity is a relatively small genome, roughly 1.7 megabases, containing approximately 1500 open reading frames (ORFs)[17–19]. Notably, its low GC content of less than 40% contributes to shaping its unique genomic make-up. One of the most striking features is the limited complexity of its transcriptional machinery and regulatory apparatus compared to other bacteria, with only 17 transcriptional regulators (TRs)[20,21]. Unlike *Escherichia coli*, an exemplary Gram-negative bacterium whose transcriptional machinery enlists an RNA polymerase (RNAP) of five subunits (α2ββ'ω) and seven sigma factors for promoter recognition—*H. pylori*'s RNAP core enzyme has its β and β' subunits fused into a single ORF, and only three sigma factors are encoded in the *H. pylori* genome, σ^{80} (RpoD), σ^{54} (RpoN), and σ^{28} (FliA)[22]. Among these, σ^{80} primarily facilitates the transcription of most genes, whereas σ^{54} and σ^{28} modulate the transcription of flagellar genes[6,21,23]. Transcriptomic analyses have revealed additional differences in promoter architecture, with unique features of σ^{80}-regulated gene promoters[24]. The majority of TRs in *H. pylori* are two-component systems (TCSs), which are ubiquitous signal transduction systems involving a membrane-bound histidine kinase (HK) and a cytoplasmic response regulator (RR)[25]. The four complete two-component systems (TCSs), FlgRS, ArsRS, CrdRS, and CheYA, enable *H. pylori* to adapt to various environmental conditions including motility, chemotaxis, acid acclimation, and copper[26–29]. In addition, two orphan response regulators, HP1021 and HP1043, that function independently of HKs, are involved in the relatively simple transcription system of the bacterium[22,24,30]. HP1021 is a redox switch regulator contributing significantly to the bacterium's oxidative stress response[31–33]. While HP1043 appears to be a master regulator governing essential cellular processes[34,35]. Additionally, four standalone TRs are encoded by the H. pylori genome, involved in metal ion homeostasis and stress responses[36,37]. The paucity of traditional transcription factors in *H. pylori* is thought to be a result of reductive evolution[20]. Its genome and regulatory framework embody a delicate balance between simplicity and efficiency. The bacterium's restricted niche in the human

gastric mucosa, coupled with a lack of competition from other microorganisms compared to other biological environments, has led to the loss of certain regulatory elements. Although *H. pylori*'s regulatory toolkit may appear small, its ability to control genes extends beyond the known TRs. Differential RNA-seq of *H. pylori* primary transcriptome has identified extensive antisense transcription and at least 60 small RNAs, a number comparable to that found in *E. coli* when adjusted for genome size[24,38,39]. Therefore, it is plausible that *H. pylori* may compensate for its limited repertoire of TRs through alternative transcriptional regulation mechanisms, using antisense transcription, RNA-binding proteins, and small RNAs to fine-tune gene expression[23,40,41]. Taken together, these elements suggest an intricate approach to transcriptional and post-transcriptional control, providing *H. pylori* with the tools to rapidly adapt to changing environments and adverse conditions. The composition of the promoter regions is another example of *H. pylori*'s distancing from other species. Unlike *E. coli*, where the -35 and -10 promoter elements contribute to transcription initiation*, H. pylori*'s σ^{80}-dependent promoters feature an extended -10 motif and an AT-rich sequence upstream of the -14 position[24,42]. This unique configuration highlights the bacterium's adaptive strategy to regulate gene expression in its specialised gastric environment.

1.3. The orphan response regulator HP1043

The orphan regulators identified in *H. pylori*, HP1021 and HP1043, differ from the typical structures found in other bacteria, raising interesting questions about potential alternative activation mechanisms, which require thorough validation[43,44]. HP1043, a central figure in *H. pylori* regulatory machinery, is an orphan response regulator that belongs to the OmpR/PhoB family of response regulator (RR) transcription factors based on its DNA-binding domain, characterized by a winged helix-turn-helix (wHTH) motif[25,45]. Typically, phosphorylation by a cognate histidine kinase (HK) induces dimerization of this class of regulators, enhancing their affinity for target DNA. However, HP1043 diverges from the other regulators as it lacks the associated HK and hence it is termed “orphan" RR. In addition, its receiver domain is

degenerate since it lacks the conserved residues essential for the phosphorylation and it is sometimes labelled "atypical"[30,46,47]. Yet, HP1043 can bind to its target genes without the need to be activated. The molecular topology of HP1043, as revealed by NMR, mirrors that of the OmpR/PhoB family[44,48]. The regulator is mainly divided into two functional domains: an N-terminal domain for dimerization and a C-terminal domain for binding to DNA, connected by a flexible linker. The dimerization domain showcases an α/β/α sandwich fold, with intricate interactions stabilizing the dimeric form. The DNA-binding domain, on the other hand, comprises a helix-turn-helix motif responsible for DNA recognition. In solution, HP1043 exists as a symmetric dimer in equilibrium with its monomeric form[34,47]. The HP1043 regulon has been mapped using chromatin immunoprecipitation-sequencing (ChIP-seq), revealing its essential role in regulating *H. pylori*'s genome expression[34] (Figure 1A). Gene ontology analysis emphasized the central involvement of HP1043 in a multitude of vital functions for the bacterium, revealing its profound impact on fundamental cellular processes ranging from motility and virulence to DNA repair and metabolism. The regulator operates on genes linked to the flagellar motor switch, chemotaxis, bacterial cell envelope, DNA replication, repair, and recombination, translation, post-translational modifications, protein turnover, and coenzyme transport and metabolism. Interestingly, HP1043 has shown the regulation of its own transcription, binding to its promoter and acting as a transcriptional activator[35,49]. Furthermore, it is believed that the HP1043 regulon is also involved in transitioning from a spiral to a coccoid shape in specific environmental conditions[49,50]. The shift in morphology appears to be a biological process initiated by the bacterium as a protective mechanism against adverse conditions, a "viable but nonculturable" state which has also been observed in other bacterial species[33,51]. This contradicts previous beliefs that the coccoid form is a non-viable state of *H. pylori*. A significant portion of its binding sites were found to be located in promoter regions, consistent with its role as a TR[34]. Nevertheless, some binding sites were also identified within protein-coding sequences and intergenic regions, suggesting diverse regulatory functions. The target promoter regions display the HP1043 binding site situated directly upstream of the -10 box, in line with the typical pattern of genes regulated

by σ^{80}. The binding sites overlap two AT-rich stretches that compensate for the lack of the conserved -35 promoter element in *H. pylori*[34,35]. This particular arrangement suggests that HP1043 may function as a transcriptional activator, as proposed by Browning and Busby in 2016[52]. *In vitro* transcription studies utilising two target promoters (P_{hp1227} and P_{hp1043}) have demonstrated an inclination towards up-regulation by HP1043 direct control[34,35]. Furthermore, an HP1043 DNA-binding domain (DBD) mutation, causing enhanced DNA affinity *in vitro*, provoked an increase in transcription for a few regulated promoters *in vivo*[53]. The consensus binding sequence for HP1043 has been delineated as a repeat of two TTTAAG hexamers, separated by a fixed 5 bp spacer (Figure 1B). Mutagenesis experiments have further refined our understanding of the sequence's importance for recognition by the dimeric HP1043, going beyond the classic sequence conservation analysis[35,49]. *In vitro* experiments have shown that the binding of HP1043 was most compromised by the mutations on the first hemisite of nucleotides (in particular A1F, A2F, and GF), but also by a mutation of four out of six nucleotides (T2S, T3S, A1S, A2S) of the second hemisite, despite being less conserved[35,49]. Thus, a consensus sequence based on the nucleotides relevant to the HP1043 binding could be stated as tttAAG-5bp-tTTAAg, with the most critical bases presented as capital letters[34,35]. The mutagenesis results also demonstrate an asymmetry in the recognition of the two hemisites of the consensus sequence by HP1043. Transcription of the *hp1043* gene is modulated by a σ^{80} promoter, it peaks during the exponential growth phase and diminishes as the bacterium enters the stationary phase[34,54]. HP1043 does not require phosphorylation in response to stimuli for its function as its receiver domain is degenerate and lacks the typical phosphorylation site[53,54]. The weaker DNA binding affinity observed *in vitro* for recombinant HP1043, compared to other *H. pylori* regulators, likely indicate a post-translational modifications of the regulator[50,53]. However, such modifications and regulations as well as the mechanisms through with HP1043 senses and responds to environmental stimuli remain not clear. The decreased *hp1043* transcription levels detected in stationary cultures might be linked to various environmental factors, including urea, low pH, metals, and AGS gastric epithelial cells as determined by real-time PCR

assays[49,53]. Moreover, the morphological shift to a coccoid form is also believed to be a result of stress response against adverse environmental conditions that involves HP1043[34,51,55]. On the other hand, the exposure to various environmental stresses, including heat shock, osmotic or acid shock, elevated iron and nickel concentrations did not affect the transcriptional level of *hp1043*[35].

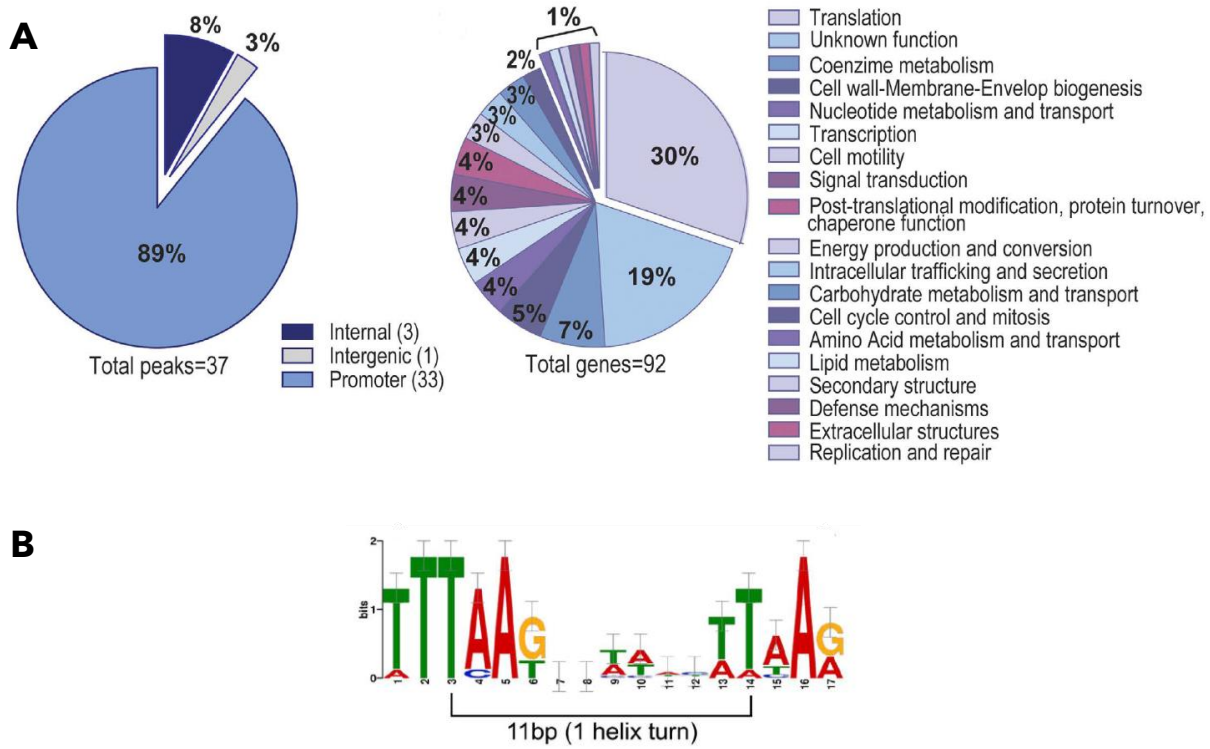

Figure 1: (**A**) Genome-wide binding analysis of HP1043; Pie charts representing the positioning of the HP1043 binding sites relative to the genes identified through ChIP-seq analysis, and a gene ontology study of HP1043 binding sites on its targets classified based on their function. (**B**) Sequence logo of HP1043 consensus binding sequence derived from alignment analysis of HP1043 binding to validated target promoter regions. The height of each letter corresponds to the relative conservation of each base. Adapted from Pelliciari et al., 2017.

1.4. Targeting the transcriptional regulator HP1043

Conventional treatments for bacterial pathogens are facing increasing difficulties in treating bacterial infections due to the rampant rise in antibiotic resistance and the decline in new antibiotic discovery efforts[4,12]. Recent studies have explored the possibility of targeting bacterial transcriptional and post-transcriptional regulators to enhance the development of new antibacterial strategies[56]. In this sense, the modulation of gene expression to adapt to environmental changes and establish

successful infections can be exploited for precise and innovative antimicrobial approaches. The mechanisms involved in regulating gene transcription in bacteria include DNA-binding regulatory proteins and small regulatory RNAs (sRNAs), among other methods[57]. Essential TRs are attractive targets for the development of novel antibiotics[14,55]. Altering the activities of these regulators results in the modified expression of pivotal genes for cell survival. In addition, considering that TRs do not have eukaryote homologous counterparts, their targeting allows for selective new antimicrobial therapeutics[58]. Nonetheless, it is crucial to comprehend these regulatory mechanisms in the struggle to develop new antibacterial drugs. The regulation played by HP1043 appears to be crucial for cell viability and fitness, a prerequisite for a successful infection, but it remains enigmatic[34]. Efforts to modulate its protein levels have faced complex challenges. The orphan RR gene cannot be deleted, nor can the amount of protein be regulated through conventional methods, as its knockout and inhibition profoundly alter the expression of crucial cellular processes[35,56]. This aspect poses challenges for researchers and makes HP1043 a promising candidate to develop novel antibacterial strategies. Moreover, targeting a TR that controls a cluster of fundamental genes will be the first example of a multitargeting approach against *H. pylori*.

1.5. Peptide Nucleic Acid

Peptide Nucleic Acid (PNA) constitutes an innovative class of synthetic molecules, which has gained substantial attention in the field of antimicrobial research by virtue of its adaptable gene knockdown activity[59,60]. Their distinct structure (Figure 2) makes them resistant to nucleases and proteases, thereby enhancing stability in biological environments. PNA's neutral pseudo-peptide backbone confers their high binding affinity with complementary RNA sequences, enabling the use of shorter oligomers, typically 8-12mers, for precise sequence targeting[61,62]. As with other antisense agents, PNAs possess the capability to selectively inhibit the expression of specific target genes.

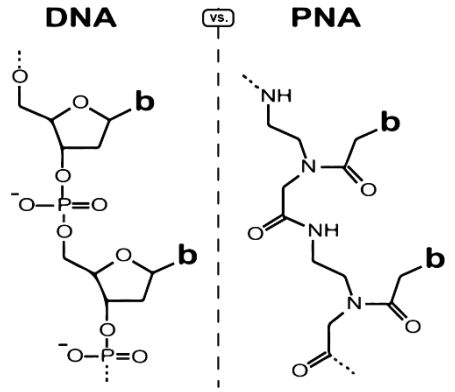

Figure 2: Chemical structure of a PNA oligomer compared with that of DNA. b indicates the nucleobases. Adapted from Good and Nielsen, 1998.

Normally, antisense agents operate via distinct mechanisms, primarily mRNA degradation through RNase H activation or steric hindrance of mRNA translation. In the case of PNA, the oligomer does not activate RNaseH and seems to function mainly by inhibiting translation[60]. Nonetheless, some studies indicate coexisting mRNA decay due to the blockade of translation. Their design involves complementarity to the translation start site of target mRNAs, thereby obstructing ribosome binding and initiation of translation. Several studies identify the start codon region and the Shine-Dalgarno motif as particularly sensitive to silencing activity, rendering the region a prime target for such antisense compounds[63-65]. When targeting essential genes, PNAs can affect vital processes and arrest bacterial growth or induce bacterial death, emphasizing the importance of target gene selection and positioning within the sensitive region for inhibition[60]. In the last decade, PNAs have exhibited substantial antimicrobial potential, particularly demonstrated against uropathogenic *Escherichia coli* (UPEC), a highly clinically relevant pathogen[66,67]. The targeting of essential genes, such as *acpP* involved in fatty acid biosynthesis, has shown potent bactericidal effects across various bacterial species, including *E. coli* and *Salmonella enterica*. Moreover, PNAs' effect goes beyond single gene knockdown, as RNA-sequencing assays indicate a significant effect on target mRNA levels and a reshaping of the bacterial transcriptome[67]. The optimization of the length of PNAs is an active area of research as shorter PNAs are

more readily taken up by cells, while longer ones possess superior binding affinities, with an optimum at 10 nucleobases for exhibited antisense activity[61,65,68]. The optimum length of PNAs is determined by molecular interactions that lead to high mRNA binding affinity and efficient bacterial uptake. Indeed, a major challenge in PNA research lies is their uptake by bacterial cells, with the inner membrane and lipopolysaccharide (LPS) layer acting as main barriers and reducing PNA uptake efficiency[69]. To enhance intrabacterial delivery, PNAs are frequently conjugated to bacterial-penetrating peptides (BPPs), cationic peptides which facilitate the crossing of the bacterial envelope[61,65,66]. BPPs have proven effective in enhancing PNA uptake, improving its gene knockdown efficacy. These BPP-PNA conjugates differ from membrane-disruptive cationic peptides, as their target is cytoplasmic. The efficiency of BPPs varies with the lipid composition of the membrane, making their efficacy species-specific. Compared to traditional antibiotics, BPP-PNA conjugates are significantly larger, around 5kDa, and also somewhat larger than most naturally derived antimicrobial peptides. Despite their size, it's unlikely that porins are involved in transporting them over the outer membrane[59]. This is supported by the fact that no porin-mediated resistance mechanisms have been identified for PNA-peptide conjugates. However, specific transporters can be involved and required for PNA translocation across the inner membrane[61,66]. A few mechanisms, both active and passive, were identified as responsible for an effective uptake of H-$(KFF)_3$K conjugates. Particularly, the SbmA transporter protein has been demonstrated to play a key role in their passage through the inner membrane, as Δ*sbmA E. coli* strain was essentially immune to antisense PNAs[68]. Among notable carrier peptides, H-$(KFF)_3$K stands out, typically linked to PNAs via an ethylene glycol bridge (eg1). It has been successfully used against a range of bacteria, including *E. coli*, *Staphylococcus aureus*, *Klebsiella pneumoniae*, *Mycobacterium smegmatis*, *Streptococcus pyogenes*, and *Acinetobacter baumannii*[64,67]. Effective carriers should exhibit low toxicity to both bacteria and host cells, along with minimal haemolytic activity. The intact peptide is crucial for uptake but not for intracellular antisense activity, and full-length BPP such as H-$(KFF)_3$K can spontaneously pass the inner membrane[66]. However, the peptide H-$(KFF)_3$K is unstable and gets degraded before reaching the

inner membrane by proteases in the bacterial culture medium and inside the bacteria[66,69].The stability to metabolism as well as the transporter-mediated uptake were then addressed by designing more stable transporter-independent cationic peptides. D-arginine-rich BPPs, such as H-(dR-eg1)$_6$ and H-(dR-eg1-dR)$_4$, have attracted attention due to their enzymatic stability and distinct uptake mechanisms[70]. Recent findings suggest that these peptides do not rely on the SbmA transporter, with an energy-dependent uptake mechanism linked to the high membrane potential observed in bacterial cells[69]. This aligns with the "self-promoted uptake" model proposed by Hancock and Chappel (Hancock and Chapple 1999). However, the precise transit mechanisms for PNAs attached to d-arginine-rich carrier peptides across the inner membrane remain partially unknown, with significant differences documented between mammalian and bacterial cells, and within different bacterial species. Ongoing research is exploring the synergistic effects of combining lipid A synthesis inhibitors with BPP-PNA conjugates, as LPS appears to present a challenge to d-arginine-rich BPPs for effective uptake. Diaminobutanoic acid (DAB) and diaminopropanic acid (DAP) dendrons have been also studied as delivery carriers for PNAs[68]. In particular, DAB-PNA conjugates have exhibited specific antisense antimicrobial activity targeting essential genes, with uptake independent of the SbmA transporter. Additionally, their high stability in human and mouse serum, low toxicity to human cells, and propensity for some bacterial strains suggest their potential for therapeutic applications, although with certain limitations[67]. PNAs present encouraging prospects for producing accurate antimicrobial agents to enhance eradication rates, combat antimicrobial resistance, and diminish adverse effects on the regular microbiota.

1.6. Innovative drug discovery, from drug repositioning to co-crystallization

Drug repositioning, also known as drug repurposing, is a relatively recent approach in drug discovery that involves repurposing existing and approved drugs for new therapeutic applications[71]. This strategy offers significant advantages, such as

reduced development costs and shorter timelines, leveraging already approved and de-risked compounds[72]. Drug repositioning is aided by high-throughput virtual screening (HTVS), which can further reduce the time associated with experimental screening[35,73]. HTVS enables the screening of large libraries of existing compounds, such as those containing FDA-approved molecules and NIH clinical collection. Subsequently, molecular dynamics (MD) simulations can be incorporated to offer dynamic insights into the molecular interactions between the screened compounds and their intended targets, thereby facilitating an understanding of the mechanisms behind the experimental results[74]. Hence, when testing drugs on new targets using a combination of computational and *in vitro* methods, the number of compounds required for *in vivo* testing is minimized[72]. When the strategy here described is combined with validated high-resolution structural data of the target, such as HP1043 in this case, it is possible to quickly identify new methods of specifically interfering with our major bacterial TR. Previous experimental data and the available NMR structure of HP1043 allowed for the generation of a docking model of the protein with DNA[48] (Figure 3). The resultant model along with single amino acid substitutions and *in vitro* binding assays have revealed an interaction between specific HP1043 dimer residues and one of its target DNA sequences, engaging in a head-to-head conformation that encompasses both the major and minor grooves of the DNA[35].

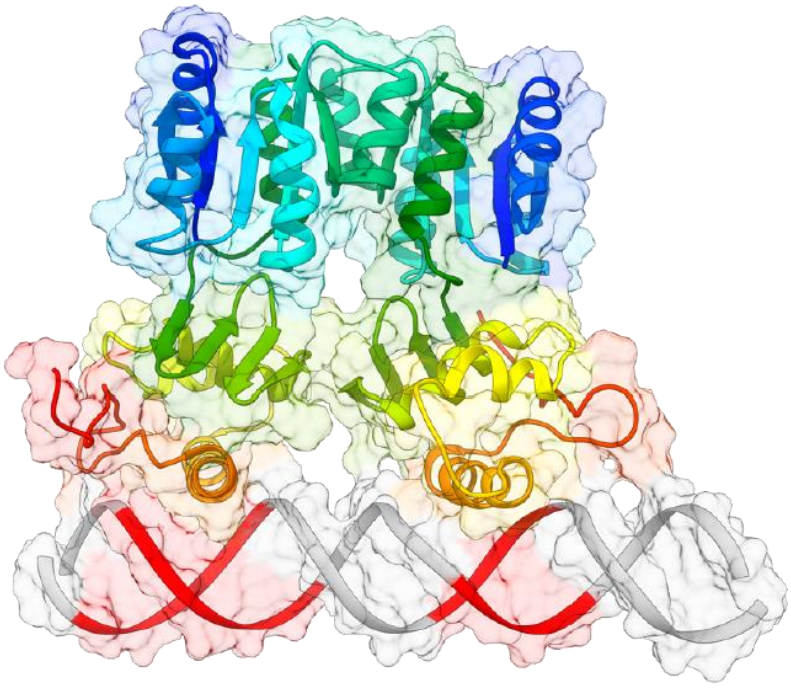

Figure 3: HP1043-P_{hp1227} docking model. HP1043-DNA interaction model showed as ribbon and surface. HP1043 monomers are displayed in rainbow, the DNA in grey, and binding nucleobases in red. Adapted from Zannoni et al., 2021.

Based on *in vitro* high-throughput screening of the Prestwich Chemical Library for small FDA-approved molecules, a recent investigation aimed to identify candidates capable of binding to key sites in HP1043, resulting in the suppression of its biological function[55]. In particular, a small cluster of flavonoids, bioactive compounds produced by several plant species and involved in oxidative stress response, was found to bind to the TR in sensitive DNA binding sites[53]. Four of these flavonoids were seen to hinder DNA binding activity in vitro and have displayed bactericidal effects towards *H. pylori*, with chrysin and hesperetin being the most effective in combination with antibiotics. Flavonoids appear to exhibit multifactorial antimicrobial activity by targeting different molecular components within pathogens[13]. However, these precise mechanisms of action remain elusive, with proposed mechanisms encompassing interference with bacterial DNA synthesis, cytoplasmic membrane permeability, and inhibition of bacterial metalloenzymes[75,76]. This approach could expand perspectives on drug repositioning in the exploration

of innovative antimicrobials targeting bacterial TRs and allow for data-driven decisions that ultimately increase the likelihood of identifying a successful "repurposed" candidate. A second approach that has been investigated lately is co-crystallization, a technique used in pharmaceutical research to enhance chemical and pharmacological properties of active pharmaceutical ingredients (APIs)[77,78]. This crystal engineering technique possesses a range of advantages that make it a promising strategy in the development of new drug formulations and the improvement of the existing ones. The basic idea behind it is the solid-state association of an active ingredient, for instance commonly used antibiotic, with a compound belonging to the GRAS (generally recognized as safe) family targeting a novel target, such as HP1043. Co-crystals can significantly improve the solubility of hydrophobic compounds, thus enhancing bioavailability, modify the release profile of the drug, allowing for controlled or sustained release, and reduce the toxicity profile of APIs[79,80]. Recently, scientific work has shown that crystal engineers can play a key role in the frontier of antimicrobial drug discovery, where co-crystallization has the potential to offer alternative pathways for the synthesis of new materials and the improvement of antibacterial properties[79].

2. AIM

H. pylori is a successful human pathogen that colonises the inhospitable gastric epithelium environment and rapidly develops resistance to standard therapies, drastically reducing its eradication rate[81,82]. Without effective treatment, *H. pylori* infection causes chronic gastritis, which may be clinically silent or progress to more severe diseases including atrophic gastritis, peptic ulcer and MALT lymphoma or gastric adenocarcinoma[2]. The bacterium's high prevalence and long persistence, along with the growing emergence of antimicrobial-resistant strains, have highlighted the need to develop new antimicrobial strategies to efficiently fight *H. pylori* infection. Targeting essential bacterial TRs is an emerging strategy in antibiotic drug discovery[56]. Within the limited repertoire of TRs in *H. pylori*, the HP1043 orphan response regulator emerges as a pivotal governing crucial cellular processes[34]. The intrinsic complexity of the TR renders straightforward deletion of its gene or precise modulation of protein levels unfeasible with standard molecular methods. This challenge for researchers studying HP1043 regulation also makes it a good candidate for novel antimicrobial therapies. This work aims to provide a framework for comprehending the regulatory mechanism of this *H. pylori* master regulator, using a refined gene reporter system to investigate *in vivo* HP1043 regulation on validated target genes, while exploring the therapeutic potential through precise targeting of this crucial TR[35,74]. In light of our *in vitro* analysis and *in silico* model, we then aimed to identify through drug repositioning a subset of approved compounds that interact with HP1043 and reduce its DNA binding affinity *in vitro* with a correlated antibacterial activity *in vivo*. Based on recent studies showing a repressive activity on HP1043 DNA binding, we studied the co-crystallization of flavonoids with standard antibiotics to achieve inhibition of the TR and reduce antibiotics dosage needed[55,83]. Finally, this project intended to provide a first example of a multi-targeting approach that leverages the antimicrobial potential of antisense PNAs designed for gene knockdown of the fundamental *hp1043*.

3. MATERIALS AND METHODS

3.1. Molecular Dynamics

Molecular dynamics simulations of the HP1043 dimer with and without the DNA molecule and in the presence of virtually screened ligands were performed on AMBER 18, as previously described[74,84]. Briefly, to parameterize the complexes listed, two force fields were employed: ff14SB[85] for the protein, OL15[86] for DNA, and water was treated as an optimal point charge. Then, we balanced the total charge of each complex by adding Na^+ counter ions, setting the solution molarity to 150mM with Na^+ and Cl^- ions. The energy of the complexes was first minimized for 1,000 steps, heated up to 300 K in 100 ps and followed by 50 ps of NPT equilibration. Finally, ten simulations of 10 ns each were performed using the molecular mechanics generalized Born surface area (MMGBSA) protocol. MMBPSA.py tools were used to estimate trajectory and energetic parameters[87]. We employed a second MMPBSA.py tool on 50 equally distributed frames along the joint trajectory to perform binding energy analysis on protein–ligand and protein (ligand)–DNA complexes, evaluating the solvation-free energy using the modified generalized Born (GB) model[88]. In this way, we could identify interacting residues and their classification as contacts or residues establishing hydrogen bonds.

3.2. Bacterial strains and growth conditions

In this study, bacterial culture conditions were established for various *H. pylori* strains as well as *E. coli* DH5α. *H. pylori* strains (G27, 26695, P12) were recovered from -80 °C glycerol stocks and propagated on Brucella Broth (BB) agar plates supplemented with 5% complement-inactivated fetal calf serum (FCS) and Dent's antibiotic supplement. Bacteria were grown with shaking (140 rpm) at 37°C in a water-jacketed thermal incubator with a controlled 9% CO_2 concentration and 95% humidity or in jars using Anaerocult™ C mini incubation bags (Sigma-Aldrich) which create a low-oxygen, high-CO_2 atmosphere, suitable for *H. pylori*. Liquid cultures were grown in either BB or non-cation-adjusted Mueller-Hinton Broth (nca-MHB) supplemented

with 5% complement-inactivated FCS. For *E. coli* DH5α, bacteria were cultured on Luria-Bertani (LB) agar or in LB broth. Media were supplemented with ampicillin (100 μg/mL), kanamycin (25 μg/mL), or chloramphenicol (30 μg/mL) when required.

3.3. DNA manipulation

DNA manipulations were carried out as described previously[89]. DNA amplification, restriction digestion, and ligation were performed according to the manufacturers' instructions (New England Biolabs). Plasmid DNA preparations were carried out using the NucleoBond Xtra Mini/Midi plasmid purification kits (Macherey-Nagel). PCRs were performed in a SimpliAmp Thermal Cycler (Thermo Fisher Scientific) using PCRBIO Classic Taq polymerase (PCR Biosystems) or Q5® High-Fidelity DNA Polymerase (New England Biolabs). PCR clean-up and DNA fragments extraction from agarose gel for cloning purposes were carried out with the NucleoSpin Gel and PCR Clean-up Kit (Macherey-Nagel).

3.4. Generation of *Helicobacter pylori* mutants

The reporter system was included in *H. pylori* genome through double homologous recombination of the naturally competent G27 strain as already described[90] and schematized in Figure 4. In brief, *H. pylori* was recovered from -80°C glycerol stocks and streaked in fresh BB agar plates. Freshly grown cells were then collected and streaked in tiny spots on fresh plates and grown for an additional 4 hours to stimulate the natural competence. Later, 5 μg of plasmid DNA were added onto the spotted bacteria and let incubate overnight. Mutants were selected on BB agar plates supplemented with antibiotics, according to the resistance phenotype conferred by the antimicrobial resistance cassette present in the recombinant region, the *aphA-3* kanamycin-resistance marker (Km^R) in this case. Transformants were observed after 3-7 days of incubation in jars containing Anaerocult™ C at 37 °C. All *H. pylori* mutants were checked for correct transformation by PCR and/or sequencing of isolated genomic DNA.

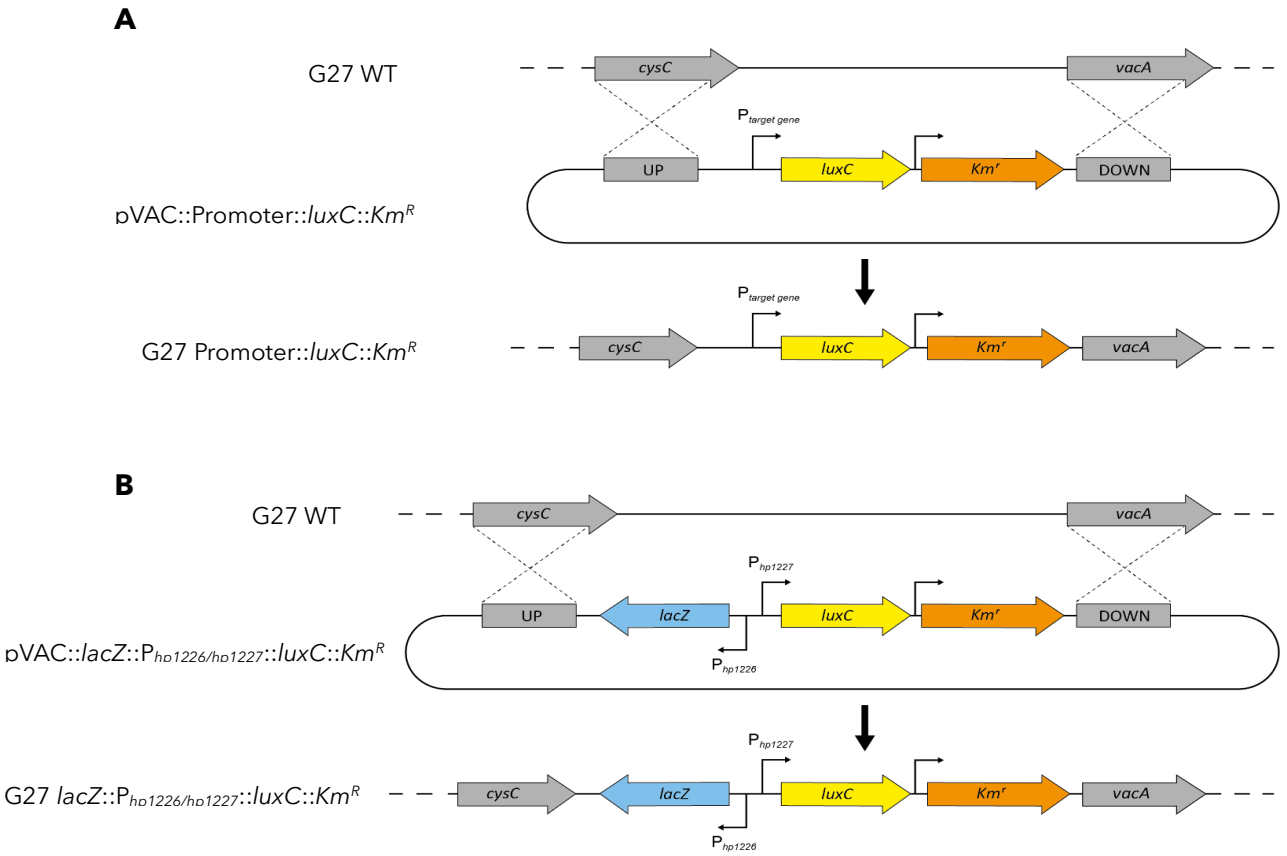

Figure 4: Schematic representation of the reporter system construction. (**A**) G27 Promoter::*luxC*::Km^R strains were obtained by double homologous recombination in the *vacA* locus, using the transforming vector pVAC::Promoter::*luxC*::Km^R. "Promoter" indicates either P_{hp1227}, P_{fldA}, P_{rpoD}, or P_{tlpB}. (**B**) Likewise, G27 *lacZ*::$P_{hp1226/hp1227}$::*luxC*::Km^R strain was obtained by double homologous recombination in the *vacA* locus with the transforming vector pVAC::*lacZ*:: $P_{hp1226/hp1227}$::*luxC*::Km^R. Promoter-less controls (here not represented) were obtained like the previous ones, using the two vectors pVAC::*luxC*::Km^R and pVAC::*lacZ*::*luxC*::Km^R.

3.5. Overexpression and purification of recombinant His6-HP1043

Recombinant N-terminal His-tagged HP1043 protein was overexpressed in *E. coli* DH5α cells transformed with the vector pTrc::1043 as previously described[35]. For EMSA assays, purified HP1043 was dialyzed twice against 1 x 1043 Footprinting Buffer (10 mM Tris-HCl pH 7.5; 50 mM NaCl; 10 mM $MgCl_2$; 1 mM DTT; 0.01% Igepal CA-630; 10% glycerol). Protein purity was assessed by SDS-PAGE and the concentration of protein preparations was evaluated by Bradford colourimetric assay (Bio-Rad) and NanoDrop® (Thermo Fisher Scientific).

3.6. RNA isolation

H. pylori was grown in liquid culture with gentle shaking as previously described and three growth samples were harvested at different growth phases (exponential, late exponential, and stationary). Right after, cells were mixed in stop buffer (95% EtOH, 5% phenol) and pelleted down at 5500 x g for 10 min at 4°C and total RNA was extracted with TRI Reagent™ (Thermo Fisher Scientific), according to the manufacturer's protocol. Total RNA samples were stored at -80°C in a precipitation mix (2V EtOH 100% and 0.1V sodium acetate 3M pH 5.2).

3.7. qRT-PCR analysis

qRT-PCR analyses were performed on a CFX Connect Real-Time System (Bio-Rad) using diluted cDNA samples synthetized as previously described. In brief, samples were treated with Thermo Scientific RapidOut DNA Removal Kit (Thermo Fisher Scientific) according to the manufacturer's protocol to remove contaminations of genomic DNA. Then, 500 ng of DNA-free total RNA were incubated with 100 pmol of random hexamer (Thermo Fisher Scientific) at 65°C for 5 minutes, followed by reverse transcription reaction with 200 U of RevertAid Reverse Transcriptase (Thermo Fisher Scientific), following manufacturer's protocol. qRT-PCR analyses of the cDNA samples were carried out using PowerUp™ SYBR™ Green Master Mix (Thermo Fisher Scientific) and 400 nM oligonucleotides (lux_RTR/lux_RTF). Gene transcription levels were estimated by applying the ΔΔCt method[91], and the *16S* rRNA gene was used as an internal reference.

3.8. Antimicrobial activity tests against *Helicobacter pylori*

In the beginning, overnight bacterial cultures were diluted to an OD_{600nm} = 0.2 and let grow till reaching OD_{600nm} = 0.6 (corresponding to 5 × 10^7 CFU/mL) in a CO_2-controlled humidified incubator (9% CO2) at 37 °C with shaking (140 rpm). Minimum inhibitory concentration (MIC) and minimum bactericidal concentration (MBC)

assays to determine the antibacterial activity of screened ligands and co-crystals against *H. pylori* were performed according to the CLSI protocol with slight modifications. The MIC was assessed by the broth microdilution method, testing all solutions/suspensions in parallel on two different strains of *H. pylori*: G27 and 26695. In brief, compounds, co-crystals, and physical mixture were prepared in 11 progressive concentrations ranging from 512 to 0.5 µg/mL. For co-crystals, solutions and dispersions were prepared in physiological solution (0.9% NaCl) to a final concentration of 2 mg/mL, while physical mixtures were prepared by mixing drug dispersion/solution and flavonoid dispersion in stoichiometric ratios, representing those of co-crystals. For screened drugs, either physiological solution or DMSO was used to solubilize the compounds to a final concentration of 2 mg/mL. The MIC assay was carried out using a 96-well microtiter plate and the two-fold serial dilutions method. Secondly, bacteria diluted in the same supplemented broth medium were added in each well to a final concentration of 1 x 10^5 CFU/mL. Negative controls were used to verify that the compound solutions/suspensions were not contaminated, while a positive control was added to check for bacterial growth and fitness. DMSO and physiological solution were included as controls. Plates were incubated in jars in the presence of Anaerocult™ C mini incubation bags at 37 °C with shaking (200 rpm) and examined visually after 48h. Then, MIC values were defined as the lowest concentration of compound that inhibited the visible growth of bacteria. For MBC determinations, each well around the MIC was diluted twice to a final 1:1000 ratio in BB and 10 µL aliquots were spotted on supplemented BB agar and incubated for another 48h in a 9% CO_2 incubator at 37 °C. MBC was defined as the lowest concentration that prevented the growth of ≥99.9% of *H. pylori*. Each experiment was performed three times to confirm the results.

To evaluate the antibacterial activity of PNA-peptide conjugates, MIC was determined as previously described by Goltremann and Nielsen[92], with a few modifications. *H. pylori* strains inoculated in nca-MHB with 5% FCS and incubated in a CO_2-controlled (9% CO_2) humidified incubator at 37 °C with shaking to reach an optical density OD_{600nm} = 0.6 (corresponding to 5 x 10^7 CFU/mL). Afterwards,

bacteria were diluted in nca-MHB with 5% FCS to achieve a concentration of approximately 5 x 10^3 CFU/ml. For the MIC assay, 180 µl of the bacterial culture was dispensed into a 96-well low-bind microtiter plate, followed by the addition of 20 µl of each peptide-PNA conjugate solution in the first wells. Through the broth microdilution method, PNA−peptide conjugates were tested at 0.125, 0.25, 0.5, 1, 2, 4, 8, 16, and 32 µM. After 48 hours of incubation at 37°C with shaking (200rpm) in jars with Anaerocult™ C mini bags, the MIC value was determined as the lowest concentration of peptide-PNA that inhibited visible bacterial growth. Internal base mismatches of PNA sequences were employed for gene silencing control. HP1043 expression after PNA treatment was examined by western blotting with a custom anti-HP1043 polyclonal antibody (Biotem).

3.9. Checkerboard assay

Potential antimicrobial synergistic effects between selected compounds and conventional antibiotics were assessed by the checkerboard assay according to established protocols[55]. To achieve this, twofold serial dilutions of these compounds were prepared in BB supplemented with 5% FBS using microtiter plates. One substance was diluted along the rows of the first plate, while the other was diluted along the columns of the second plate. Following this, equal volumes of both gradients were mixed in a third microtiter plate. Subsequently, a freshly grown *H. pylori* adjusted to 1 × 10^5 CFU/ml in BB + FBS was inoculated into this mixture. Bacteria were incubated at 37°C for 48 hours in a CO_2-controlled humidified incubator (9% CO_2). Microbial growth was evaluated visually. The fractional inhibitory concentration index (FICI) was determined as FIC_A (MIC_A in the presence of B/MIC_A alone) + FIC_B (MIC_B in the presence of A/MIC_B alone), in which A and B indicate distinct antimicrobial agents. The interaction kinds were determined by FICI values of ≤0.5 for synergistic, 0.5 < FICI ≤ 1 for additive, 1 < FICI ≤ 4 neutral, and FICI > 4 for antagonist.

3.10. Electrophoretic Mobility Shift Assays

The DNA-binding activity of the recombinant HP1043 in the presence of a specific DNA probe was assessed by EMSAs as already described[74]. In brief, 189 to 241-base pair (bp) promoter regions of *hp1227, rpoD, fldA,* (strain 26695 annotation; P_{hp1227}, P_{rpoD}, P_{fldA})[18] including the wild type HP1043 binding consensus sequence and their relative mutants (A1F, T3S) were amplified from pVAC-Promoter-*luxC*-Km^R by PCR with oligos Vac_EMSA_F and luxC_EMSA_R and used as a target sequence of HP1043. A 127bp sequence obtained through PCR amplification with oligos 16S_RTF and 16S_RTR was used as a non-specific control. EMSA assays were performed by mixing the recombinant His-tagged HP1043 with approximately 10 ng of target promoter probe and 10 ng of non-specific DNA probe in a 20 µL reaction volume containing 1x binding buffer (10 mM Tris-HCl pH 7.2, 70 mM NaCl, 30 mM KCl, 100 µg/ ml BSA, 5 mM DTT, and 10% glycerol). For DNA binding interference assays, putative ligands were added to final concentrations of 1, 0.5, 0.2, 0.1 and 0.05 mM. Binding assays with DMSO (6% (v/v)) or H_2O instead of inhibitors and 1 x binding buffer instead of the protein were included as controls. The reactions were incubated at room temperature for 30 min and then separated on a pre-run 6% non-denaturing polyacrylamide gel 0.5 × running buffer (45 mM Tris pH 7.2 and 45 mM orthoboric acid) at 90 V for 75 min, using a Mini Gel Tank apparatus (Invitrogen). DNA bands were stained with 1 × ethidium bromide and visualized using a Gel Doc XR+ image analyzer (BioRad). The binding affinity to wild type and mutated targets of the recombinant HP1043 was assessed by employing increasing protein concentration (C_f : from 0.25 to 8 µM), and 2 µM was chose to test the DNA binding inhibition of screened ligands.

3.11. *In vitro* translation reactions and *in vivo* expression

For *in vitro* translation of HP1043 in the presence of PNAs, the PURExpress® *in vitro* Protein Synthesis Kit (New England Biolabs) was used following the manufacturer's instructions with minor modifications. To detect the protein production and its inhibition by PNAs, the ribosome binding site (RBS) and the first 221 nucleotides of

the *hp1043* gene were fused in frame with GFPuv*(F64L, S65T), in a p411 vector for fluorescence detection. Simultaneously, a full-length gene was inserted in the same vector for western blot detection after the induction in *E. coli* DH5α. Both plasmid and mRNA, produced with MEGAscript T7 transcription kit (Invitrogen), were used for *in vitro* translation reactions. The reactions required a T7 promoter, that was introduced ahead of *H. pylori* RBS, and a strong terminator. Variable concentrations of BPP-PNA conjugates were used, 200 nM, 1 μM, and 5 μM, corresponding to 50:1, 250:1, and 1000:1 mole ratios of BPP-PNA:DNA, while, *in vitro* reactions with RNA, 100:1 and 10:1 mole ratios of BPP-PNA:RNA were assessed. Briefly, the final volume of each *in vitro* translation reaction was set to 5 μL, each containing 2 μL Solution A, 1.5 μL Solution B (from the PURExpress kit, New England Biolabs), 20 fmol of plasmid or 100 fmol of RNA, and BPP-PNA conjugate solution at the desired concentration. The tubes were incubated for 1h at 37◦C with shaking, and then immediately placed on ice. For visualization of the in vitro translated protein, 100 μL of PBS were added to the samples and the whole content was transferred on a 96-well microplate for fluorescence reading. The fluorescence intensity was measured on a fluorescence microplate reader. *In vivo* HP1043 expression after BPP-PNA conjugates treatment was assessed by western blotting with a custom anti-HP1043 polyclonal antibody (Biotem).

3.12. Uptake fluorescence analysis

The BODIPY FL labelled BPP-PNAs conjugates 5509, carrying the $(KFF)_3K$ peptide, and 6256, carrying the $(R\text{-}X\text{-}R)_4$ peptide, were selected to better understand the uptake efficacy. *H. pylori* G27 and *E. coli* DH5α or DH10β were grown till the log phase. Next, bacteria were diluted to OD_{600nm} = 0.2 in nca-MHB and incubated with different concentrations of labelled PNAs for 1h in jars with Anaerocult™ C mini bags. After incubation, bacteria were washed three times in PBS and mounted on top of the agarose for microscope imaging.

3.13. Phenotype analysis

H. pylori G27 was grown at 37 °C in nca-MHB with gentle shaking until the appropriate growth phase (OD_{600nm} = 0.6, ~ 5 x 10^7 CFU/mL). Bacteria were then diluted to 5 x 10^4 CFU/mL in nca-MHB. Bacteria were then incubated with the anti-*ftsZ* PNA or the anti-*hp1043* PNA and corresponding mismatch for 12h (for anti-*hp1043* induced changes) or 24h. Bacteria were harvested, washed once with PBS, and the pellet was resuspended in 1 x PBS solution of Quinaldine Red (Sigma-Aldrich). Then, the dyed cells were washed three times with PBS and resuspended 1:50 in PBS in order to be investigated through fluorescence microscope imagining.

Table 1: Strains used in this study.

Strain	Genotype	Source/reference
H. pylori strains		
G27	Clinical isolate; wild-type parental strain	(Xiang et al., 1995[93])
26695	Clinical isolate; wild-type parental strain	(Tomb et al., 1997)
G27 *luxC*::Km^R	G27 transformed with pVAC::*luxC*::Km^R	This study
G27 P_{hp1227}::*luxC*::Km^R	G27 transformed with pVAC::P_{hp1227}::*luxC*::Km^R	This study
G27 P_{hp1227}A1F::*luxC*::Km^R	G27 transformed with pVAC::P_{hp1227}A1F::*luxC*::Km^R	This study
G27 P_{hp1227}T3S::*luxC*::Km^R	G27 transformed with pVAC::P_{hp1227}T3S::*luxC*::Km^R	This study
G27 P_{rpoD}::*luxC*::Km^R	G27 transformed with pVAC::P_{rpoD}::*luxC*::Km^R	This study
G27 P_{rpoD}A1F::*luxC*::Km^R	G27 transformed with pVAC::P_{rpoD} A1F::*luxC*::Km^R	This study
G27 P_{rpoD}T3S::*luxC*::Km^R	G27 transformed with pVAC::P_{rpoD}T3S::*luxC*::Km^R	This study
G27 P_{fldA}::*luxC*::Km^R	G27 transformed with pVAC::P_{fldA}::*luxC*::Km^R	This study
G27 P_{fldA}A1F::*luxC*::Km^R	G27 transformed with pVAC::P_{fldA}A1F::*luxC*::Km^R	This study
G27 P_{fldA}T3S::*luxC*::Km^R	G27 transformed with pVAC::P_{fldA}T3S::*luxC*::Km^R	This study
G27 P_{tlpB}::*luxC*::Km^R	G27 transformed with pVAC::P_{tlpB}::*luxC*::Km^R	This study
G27 *lacZ*::*luxC*::Km^R	G27 transformed with pVAC::*lacZ*::*luxC*::Km^R	This study
G27 *lacZ*::$P_{hp1226/hp1227}$::*luxC*::Km^R	G27 transformed with pVAC::*lacZ*::$P_{hp1226/hp1227}$::*luxC*::Km^R	This study
E. coli strains		
DH5α	supE44 DlacU169 (f80 lacZDM15) hsdR17 recA1 endA1 gyrA96 thi-1 relA1b	(Hanahan, 1983[94])

DH10β	F- mcrA Δ(mrr-hsdRMS-mcrBC) Φ80dlacZΔM15 ΔlacX74 endA1 recA1 deoR Δ(ara,leu)7697 araD139 galU galK nupG rpsL λ-	(Grant et al., 1990)

Table 2: Plasmid used in this study.

Plasmid	Description	Source/reference
pTrc::1043	Derivative of pTrcHisA expressing the HP1043 response regulator; Amp^R	(Delany et al., 2002)
pVAC::Km^R	Cloning vector, Km^R	(Delany et al., 2002)
pVCC	Vector carrying the *luxCDABE* cassette	(Vannini et al., 2014[95])
pVAC *luxC*::Km^R	pVAC::Km^R derivative containing a DNA fragment of 976 bp corresponding to *luxC* gene amplified with oligos luxF_2 and luxR from pVCC	This study
pVAC::P_{hp1227}::*luxC*::Km^R	pVAC::*luxC*::Km^R derivative containing a DNA fragment of 115 bp corresponding to Php1227 promoter amplified with oligos P1227_F and P1227_R from pLux-*p1227*_WT	This study
pLUX-*p1227*_WT	pLux derivative containing a DNA fragment of 61 bp amplified by PCR with oligos p1227Eco FW/p1227Eco RV from PBSK-p1227 WT upstream *luxCDABE* operon	(Pelliciari et al., 2018)
pLUX-*p1227*_A1F	pLux derivative containing a DNA fragment of 61 bp amplified by PCR with oligos p1227Eco FW/p1227Eco RV from PBSK-p1227 A1F upstream *luxCDABE* operon	(Pelliciari et al., 2018)
pLUX-*p1227*_T3S	pLux derivative containing a DNA fragment of 61 bp amplified by PCR with oligos p1227Eco FW/*p1227*Eco RV from PBSK-p1227 T3S upstream *luxCDABE* operon	(Pelliciari et al., 2018)
pVAC::P_{hp1227}A1F::*luxC*::Km^R	pVAC:: P_{hp1227}::*luxC*::Km^R derivative obtained by substituting P_{hp1227} with a DNA region of 115 bp corresponding to P_{hp1227}A1F amplified with oligos P1227_F and P1227_R from pLux-*p1227* A1F	This study
pVAC::P_{hp1227}T3S::*luxC*::Km^R	pVAC:: P_{hp1227}::*luxC*::Km^R derivative obtained by substituting P_{hp1227} with a DNA region of 115 bp corresponding to P_{hp1227}T3S amplified with oligos P1227_F and P1227_R from pLux-*p1227* T3S	This study
pVAC::P_{rpoD}::*luxC*::Km^R	pVAC:: P_{hp1227}::*luxC*::Km^R derivative obtained by substituting P_{hp1227} with a DNA region of 171 bp corresponding to P_{rpoD} amplified with oligos rpoD_F and rpoD_R from *H. pylori* gDNA	This study
pVAC::P_{rpoD}A1F::*luxC*::Km^R	pVAC:: P_{hp1227}::*luxC*::Km^R derivative obtained by substituting P_{hp1227} with a DNA region of 174 bp corresponding to P_{rpoD}A1F amplified with oligos rpoD_F and rpoD_A1F from *H. pylori* gDNA	This study

pVAC::P_{rpoD}T3S::*luxC*::Km^R	pVAC:: P_{hp1227}::*luxC*::Km^R derivative obtained by substituting P_{hp1227} with a DNA region of 174 bp corresponding to P_{rpoD}T3S amplified with oligos rpoD_F and rpoD_T3S from *H. pylori* gDNA	This study
pVAC::P_{fldA}::*luxC*::Km^R	pVAC:: Php1227::*luxC*::Km^R derivative obtained by substituting P_{hp1227} with a DNA region of 159 bp corresponding to P_{fldA} amplified with oligos fldA_F and fldA_R from *H. pylori* gDNA	This study
pVAC::P_{fldA}A1F::*luxC*::Km^R	pVAC:: Php1227::*luxC*::Km^R derivative obtained by substituting P_{hp1227} with a DNA region of 159 bp corresponding to P_{fldA}A1F amplified with oligos fldA_F and fldA_A1F from *H. pylori* gDNA	This study
pVAC::P_{fldA}T3S::*luxC*::Km^R	pVAC:: Php1227::*luxC*::Km^R derivative obtained by substituting P_{hp1227} with a DNA region of 159 bp corresponding to P_{fldA}T3S amplified with oligos fldA_F and fldA_T3S from *H. pylori* gDNA	This study
pVAC::P_{tlpB}::*luxC*::Km^R	pVAC:: P_{hp1227}::*luxC*::Km^R derivative obtained by substituting P_{hp1227} with a DNA region of 154 bp corresponding to P_{tlpB} amplified with oligos tlpB_F and tlpB_R from *H. pylori* gDNA	This study
pVAC::*lacZ*::*luxC*::Km^R	pVAC::*luxC*::Km^R derivative containing a DNA fragment of 427 bp corresponding to *lacZα* gene amplified with oligos lacZ_NcoI_F and lacZ_NcoI_R from pBluescript II KS (+)	This study
pVAC::*lacZ*::$P_{hp1226/hp1227}$::*luxC*::*Km*	pVAC:: P_{hp1227}::*luxC*::Km^R derivative obtained by substituting P_{hp1227} with a DNA region of 115 bp corresponding to P_{hp1227} amplified with oligos P1227_F and P1227_R from pLux-*p1227* WT	This study
p411::P_{T7}::GFPuv	Cloning vector, GFPuv*(F64L, S65T)	(Cook et al., 2018[96])
p411::P_{T7}::216-*hp1043*::GFPuv	p411::P_{T7}::GFPuv derivative containing a DNA fragment of 216 bp corresponding to a part of *hp1043* gene amplified with oligos 1043CDS_Primer Fw and 1043CDS_Primer Rev from *H. pylori* G27 gDNA	This study
pBluescript KS II (+)	Cloning vector, Amp^R	Stratagene
pBS::P_{T7}::*hp1043*::Ter	pBluescript KSS II (+) derivative containing a DNA fragment of 760 bp corresponding to *hp1043* gene and a terminator region amplified with oligos ivtr1043_Fw and ivtr1043_Rev *H. pylori* G27 gDNA	This study

Table 3: Oligonucleotides used in this study.

Primer	Sequence	*	Source/reference
LuxRTF	ATCATCCGATAACGCGCTCTT	RT	(Pepe et al., 2018[97])
LuxRTR	ACCGCCCAATTAATCGCATC	RT	(Pepe et al., 2018[97])
Vac_EMSA_Fw	GCACGATTTGGGAGAAG	E	This study
luxC_EMSA_Rev	GCCGTTAATAATGAATGAAATT	E	This study
16SRTF	GGAGTACGGTCGCAAGATTAAA	E	(Pelliciari er al., 2017)

16SRTR	CTAGCGGATTCTCTCAATGTCAA	E	(Pelliciari er al., 2017)
P1227_F	ATATCCATGGGCGGCCGCTGTATAAAATCATATTTATTTCTCTTATTTTCACTTCATTTT	C	This study
P1227_R	ATATGTCGACGCTAGCCTTATCAAAATGATCTTAAAATGATACAATTACAAGT	C	This study
rpoD_F	ATATCCATGGCAAACGCAAACAATTGAAACCC	C	This study
rpoD_R	ATATGCTAGCCCCATGCTTTCAACCAAAAG	C	This study
rpoD_A1F	ATATGCTAGCGCTTTCAACCAAAAGCTAGGTCTATAGATAAGATACACCTAATCCTCTGCTATTCTACTAAAAAATAGCTAAAATTC	C	This study
rpoD_T3S	ATATGCTAGCGCTTTCAACCAAAAGCTAGGTCTATAGATAAGATACACCTAATCCTCTGCTATTCTACTATAAAATAGCTTAAATTC	C	This study
fldA_F	ATATCCATGGTCATAAGTTTTGTTCTTATAGTGCT	C	This study
fldA_R	ATATGCTAGCTAAAGATGTTAACGCACCCG	C	This study
fldA_A1F	ATATGCTAGCTAAAGATGTTAACGCACCCGCTTTTAGCGAATGCTTGCGGGCATAGTCTAGCGCATTTAATTAAACATCTTGCTAAAAAAC	C	This study
fldA_T3S	ATATGCTAGCTAAAGATGTTAACGCACCCGCTTTTAGCGAATGCTTGCGGGCATAGTCTAGCGCATTTAATTATACATCTTGCTTAAAAAC	C	This study
tlpB_F	ATATCCATGGAGACGGGAGGACTTTGAATG	C	This study
tlpB_R	ATATGCTAGCTGAAAACGAAACAGAGAACAAAC	C	This study
lacZ_NcoI_F	ATATCCATGGCATCACCCTAATCAAGTTTTTTGG	C	This study
lacZ_NcoI_R	ATATGCGGCCGCCACCGCGGTGGAGCTC	C	This study
1043CDS_Primer Fw	TGTCTAGATTTGTTTAACTTTAAGAAGGAGAGTTGAATTACTCTTAAATGCGGGAG	C	This study
1043CDS_Primer Rev	AGCATATGAACAAAACTTAAAGCGTTTTTATCAC	C	This study
ivtr1043_Fw	GAATTAATACGACTCACTATAGGGTTGAATTACTCTTAAATGCGGGAG	C	This study
ivtr1043_Rev	AAACCCCTCCGTTTAGAGAGGGGTTAAGAATTTATTCTTCACACGCCG	C	This study

*RT=Real-Time PCR, E=EMSA, C=Cloning

Table 4: BPP-PNA conjugates used in this study.

No.	PNA Sequence	BPP	Target Position (ref. start codon)
BPP-PNA conjugates targeting ***hp1043***			
5970	TATGTGGTACG	H-(KFF)$_3$K	from -7 to +4
5972	TAGGTGTTACG	H-(KFF)$_3$K	from -7 to +4
5971	TATGTGGTACG	H-(dR-eg1-dR)$_4$	from -7 to +4
5973	TAGGTGTTACG	H-(dR-eg1-dR)$_4$	from -7 to +4
6124	ATGTGGTACG	H-(dR- eg1)$_6$	from -6 to +4
6126	ATGAGGTTCG	H-(dR- eg1)$_6$	from -6 to +4
6125	TGTGGTACG	H-(dR- eg1)$_6$	from -5 to +4
6127	TGAGGTTCG	H-(dR- eg1)$_6$	from -5 to +4
6255	CATGGTGT	H-(dR- eg1)$_6$	from -5 to +3
6256	CGTGGTAT	H-(dR- eg1)$_6$	from -5 to +3
6265	TATGACTCC	H-(dR- eg1)$_6$	from -13 to -5
6266	TACGACTTC	H-(dR-eg1)$_6$	from -13 to -5
6267	CATGGTGT	H-(dR-eg1)$_6$ and (eg1-dR)$_3$-NH_2	from -5 to +3
6268	CGTGGTAT	H-(dR-eg1)$_6$ and (eg1-dR)$_3$-NH_2	from -5 to +3
6312	TATGACTCC	H-(KFF)$_3$K	from -3 to +5
6313	TACGACTTC	H-(KFF)$_3$K	from -3 to +5
BPP-PNA conjugates targeting ***ftsZ***			
6310	TGAACCATA	H-(dR-eg1)$_6$	from -1 to +8
6311	TCAACGATA	H-(dR-eg1)$_6$	from -1 to +8
Non-specific BPP-PNA conjugates with **BODIPY FL** probe			
5509	CGATTGACGA	H-(dR-eg1-dR)$_4$	n/a
6278	GACTGCATAC	H-(KFF)$_3$K	n/a

4. Results

4.1. A reporter system for HP1043 regulation study

A profound understanding of bacterial transcriptional regulation, especially in multidrug-resistant pathogens such as *H. pylori*, can lead to novel molecular approaches and promising pharmacological strategies. The deep understanding of HP1043 offers us an interesting example that holds challenges and opportunities to test innovative approaches that target specifically bacterial TRs. This study started with the design and construction of a reporter system tailored for the deep molecular analysis of HP1043 transcription regulation. The system exploits the *luxC* gene as a reporter under the control of previously validated target promoters of HP1043. *luxC* has already demonstrated its effectiveness as a reporter gene in *H. pylori* G27[97,98]. Selected promoter regions, containing the HP1043 consensus sequence, were integrated upstream of the *luxC* reporter gene in the pVAC::*luxC*::Km^R vector, which was subsequently used to transform *H. pylori* G27, as illustrated in Figure 4. Among these promoter regions, P_{hp1227} was chosen as a positive control due to the extensive *in vitro* validation as an HP1043 target. Previous research has suggested a transcriptional activation of *hp1227* by the TR based on *in vitro* analysis[34,35]. The strain harbouring the reporter system (G27 Promoter::*luxC*::Km^R) was compared to its promoter-less reporter gene control G27 *luxC*::Km^R. The analysis of the reporter gene transcriptional level in the *H. pylori* G27 strains was conducted through RT-qPCR. Hence, relying on prior validations, the reporter system was first tested on P_{hp1227}. Figure 5A shows the transcription levels of the *luxC* gene in the promoter-containing strain in comparison to the promoter-less control strain during three distinct growth phases (exponential, late exponential, stationary). The increased *luxC* expression under the control of P_{hp1227} indicates the efficacy of our reporter system in studying HP1043 regulation *in vivo* and also the consistency with previous results obtained *in vitro*. Therefore, we decided to leverage the reporter system to deepen our knowledge of HP1043 regulation. We selected three additional promoters (P_{fldA}, P_{rpoD}, P_{tlpB}) based on the genome-wide

ChIP-seq analysis performed by Pelliciari and coworkers (2017). In particular, *tlpB* was chosen because it had been previously verified as an HP1043 target[54], despite not being listed among the 37 peaks of the ChIP-seq analysis. The choice of the promoters had also the goal of investigating the positioning of the HP1043 consensus sequence upstream of the -10 sequence, allowing for the evaluation of a potential correlation between their relative distances and the transcriptional regulation imposed by HP1043. By examining the *luxC* expression levels of the three targets (Figure 5B), we obtained preliminary insight into the correlation between divergent regulatory activity and the consensus sequence distance from the putative Pribnow box element. Both *fldA* and *tlpB* promoters exhibit a binding sequence located at a distance of 11 and 10 bp from the hypothesized Pribnow box element, respectively. In contrast, the *rpoD* promoter region presents a confirmed HP1043 consensus sequence adjacent to the -10 sequence[34]. P_{fldA}::*luxC*::Km^R exhibited a substantial increase of approximately 20-40 times in the reporter gene transcription across all the investigated growth phases. Whereas P_{tlpB}::*luxC*::Km^R displayed a modest increase in *luxC* transcription during the exponential and late exponential phases, which decreased as the bacterial growth progressed. Surprisingly, *luxC* under the control of P_{rpoD} showed a transcriptional level lower than the promoter-less one in the exponential and late exponential phases. A potential explanation for these repeatable outcomes could be a basal level of *luxC* transcription, which seems to be decreased when P_{rpoD} is introduced upstream of the gene. One speculation is that HP1043 may inhibit transcription by binding to the consensus sequence, leading to the blockage of the RNA polymerase recognition and binding to the promoter.

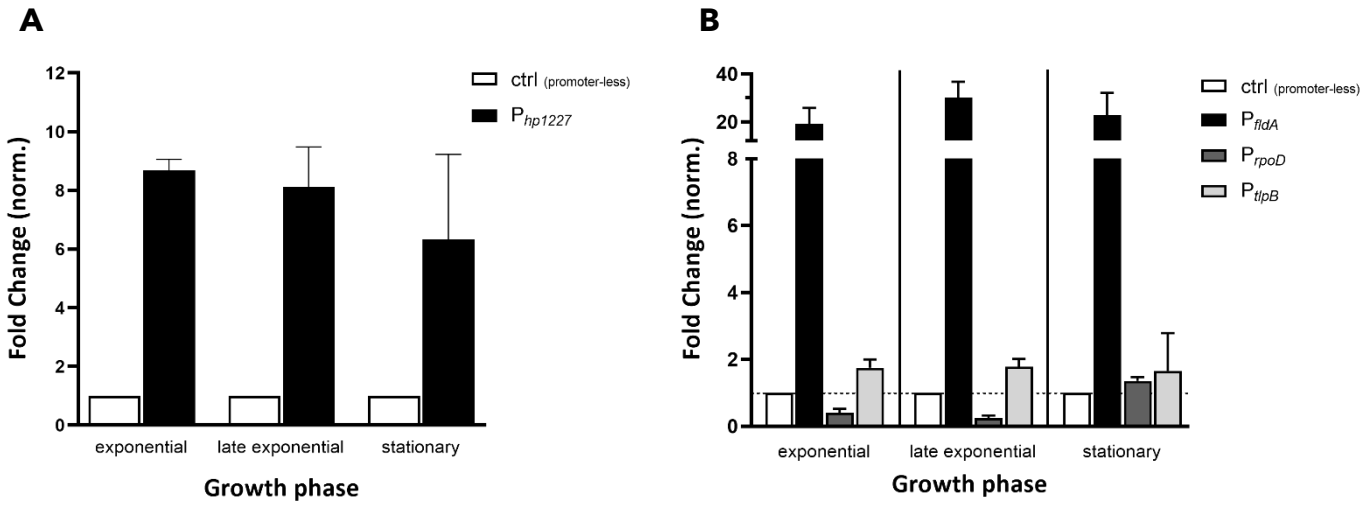

Figure 5*:* qRT-PCR analysis of the reporter system. *luxC* transcription levels are indicated as fold change. Data were normalized against the housekeeping *16S* rRNA gene and compared to basal *luxC* expression in the promoter-less control strain. *luxC* transcription levels in G27 P_{hp1227}::luxC::Km^R (in black) (**A**) and G27 P_{fldA}/P_{rpoD}/P_{tlpB}::*luxC*::Km^R (respectively in black, dark grey, and grey) (**B**) are compared to the control G27 *luxC*::Km^R (white) (**A**,**B**), in the indicated three different growth phase. The graphs represent mean data obtained from technical duplicates of three biological replicates with relative SEM.

To further investigate this hypothesis, the study of the transcriptional level of *luxC* was extended to G27 strains carrying reporter systems that harbour point mutations in either the first or second hemisite of the HP1043 consensus sequence. The choice of these mutants was based on previous mutagenesis experiments of the *hp1227* promoter assessed by DNase I footprinting and *in vitro* transcription assays[35]. These analyses highlighted the importance of specific nucleotides in both hemisites (A1, A2, and G in the first hemisite and T2, T3, A1, and A2 in the second hemisite) for HP1043 affinity to its consensus sequence (see figure 1B). In particular, the point mutation of two key nucleotides A1F and T3S in P_{hp1227} consensus sequence resulted in the loss of protein affinity to DNA (as indicated by the less protected region, Figure 6A) and reduced activation of *in vitro* transcription of the *lux* operon compared to the wild type promoter in the presence of HP1043 (Figure 6B).

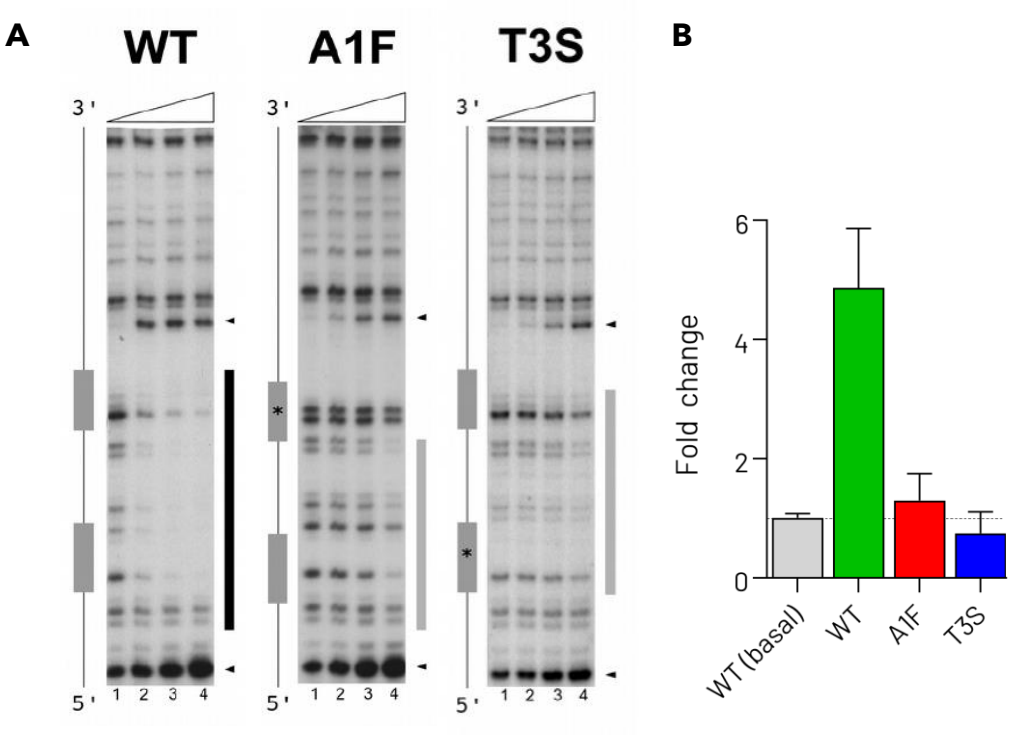

Figure 6: (**A**) DNase I footprinting experiments performed on P_{hp1227} wild type and mutants (P_{hp1227}A1F and P_{hp1227}T3S) with increasing amounts of HP1043 protein (0, 1.7, 6.6, and 13.3 μM). On the left of each experiment is reported a schematic representation of the consensus sequence, with grey boxes marking the positions of the hemisites and an asterisk to indicate the mutated nucleotide. On the right of each footprint, a black bar indicates the protected region for the wild type and grey bars the weaker protected regions. (**B**) *In vitro* transcription on *hp1227* wild type and mutated promoters positioned upstream the *lux* operon. In grey is indicated the wild type transcription level in absence of HP1043 (basal transcription level), in green the transcript level of the same construct with HP1043. The red bar reports the first hemisite mutant (A1F) while the blue bar reports the second hemisite mutant (T3S). The histogram represents mean data obtained from three technical replicates with relative SEM. Figure adapted from Zannoni et al., 2021.

Hence, P_{hp1227} was chosen as an emblematic subject for gene reporter *in vivo* analysis in virtue of the data previously obtained *in vitro* that allows for comparison[35]. The two mutants for the consensus sequence of P_{hp1227}, P_{hp1227}A1F and P_{hp1227}T3S, were generated, and they were placed upstream of the *luxC* gene in the Promoter::*luxC* system. The RT-qPCR analyses of *luxC* expression in G27 P_{hp1227}A1F::*luxC*::Km^R and G27 P_{hp1227}T3S::*luxC*::Km^R strains are presented in Figure 7. The transcriptional levels of the reporter gene significantly decreased in mutant strains during both exponential and late exponential phases compared to P_{hp1227} wild type strain. On the other hand, during the stationary phase, there were no significant transcriptional variations, aside from a minor reduction in *luxC* expression and a tendency for higher fluctuations in biological replicates. This circumstance can be ascribed to a decline

in the intracellular regulation by HP1043 in the advanced growth phase. This hypothesis is consistent with previous data reporting primer extension analysis on *hp1043*[54]. These findings consistently support the hypothesis that mutations in the HP1043 consensus sequence hinder the regulation of *hp1227* in the reporter system. Consequently, it can be affirmed that HP1043 activates *hp1227* transcription *in vivo* as well, and our *luxC* reporter system provides an efficient tool for characterizing HP1043's regulatory activity.

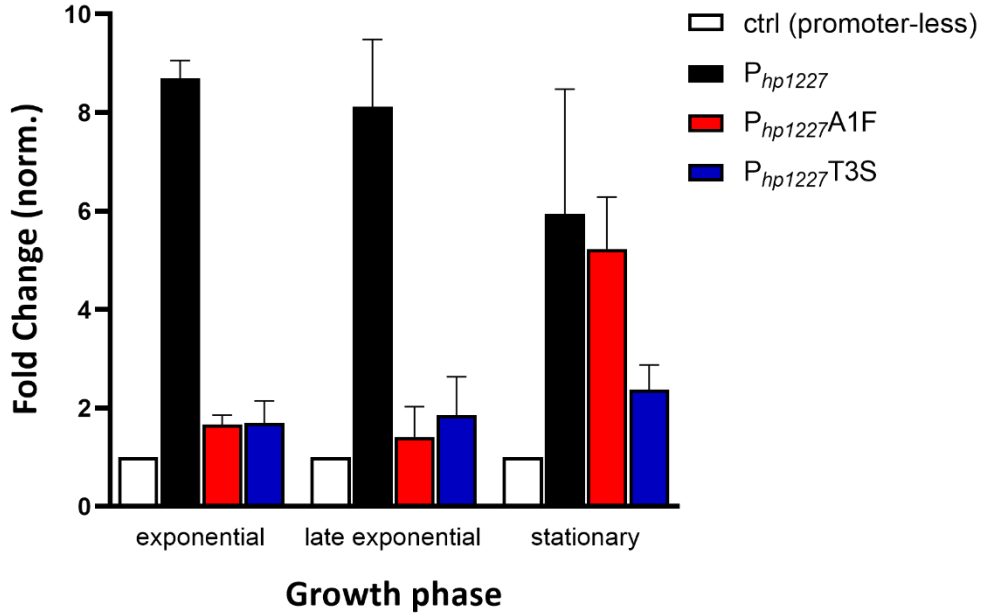

Figure 7: qRT-PCR analysis of the reporter system with *hp1227* mutated promoter. *luxC* transcription levels are indicated as fold change. Data were normalized against the housekeeping *16S* rRNA gene and compared to basal *luxC* expression in the promoter-less control strain. *luxC* transcription levels in G27 P_{hp1227}::*luxC*::Km^R (in black), G27 P_{hp1227}A1F::*luxC*::Km^R (red), and G27 P_{hp1227}T3S::*luxC*::Km^R (blue) are compared to the control G27 *luxC*::Km^R (white), in three different growth phase. The graphs represent mean data obtained from technical duplicates of three biological replicates with relative SEM.

Once confirmed the effectiveness of our reporter system, we moved on and explored further HP1043 regulatory activity in different contexts. Based on our *in vivo* analysis of other targets with a variable distance between the consensus sequence and the -10 element, specifically *fldA* and *rpoD*, we introduced the A1F and T3S point mutations in their respective promoter regions. *fldA* represents the most prevalent distribution of the consensus sequence positioning throughout the promoter region of HP1043 targets. As previously demonstrated, its expression was

higher than other targets. This suggests the presence of a strong promoter and thus modifying the consensus sequence could have a partial impact on the *in vivo* regulation of the reporter gene. Indeed, the two point mutations resulted in a minor reduction of *luxC* expression compared to the wild type strain, with a slightly more evident effect for the T3S mutant (Figure 8B). Nevertheless, the resulting lower fold changes correlated to the two point mutations recall what was seen previously in the case of *hp1227*. Data presented in Figure 8A further consolidate the prior hypothesized repression that occurs within *rpoD* regulation. It is noteworthy that the point mutations on the consensus sequence altered the presumed repression of basal transcription observed in P_{rpoD} wild type. The increase in transcriptional level of *luxC* is particularly pronounced when the point mutation is located in the first hemisite, as shown by the higher red bars in Figure 8A and represented as a red box in Figure 8C, and it is maintained in all three growth phases.

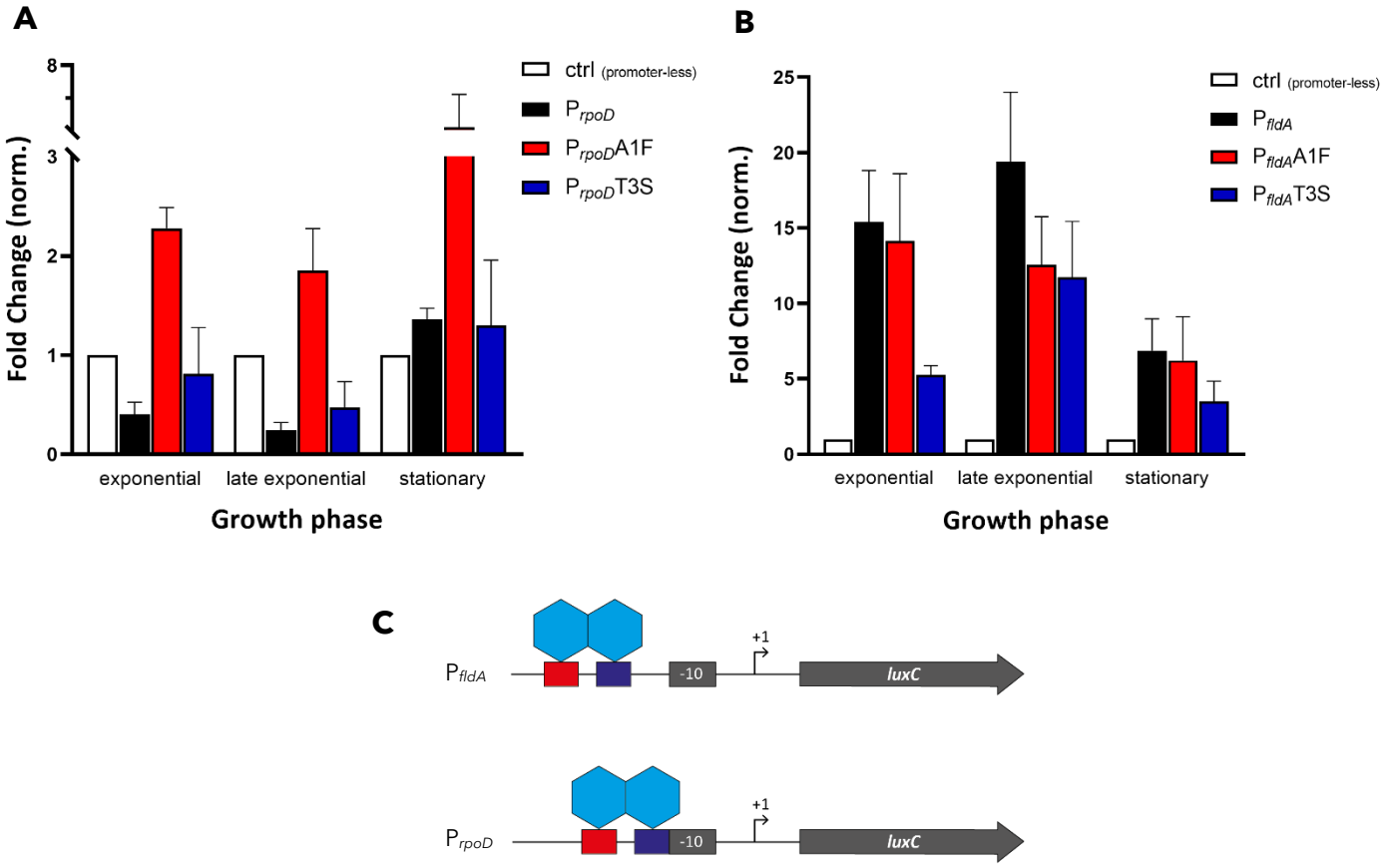

Figure 8: qRT-PCR analysis of the reporter system with mutated promoters. *luxC* transcription levels are indicated as fold change. Data were normalized against the housekeeping *16S* rRNA gene and compared to basal *luxC* expression in the promoter-less control strain. (**A**, **B**) *luxC* transcription levels in G27 P_{rpoD}/P_{fldA}::luxC::*Km*^{R} (in black), G27 P_{rpoD}/P_{fldA}A1F::*luxC*::*Km*^{R} (red), and G27 P_{rpoD}/P_{fldA}T3S::*luxC*::*Km*^{R} (blue) are compared to the control G27 *luxC*::*Km*^{R} (white), in three different growth phase. The graphs represent mean data obtained from technical duplicates of three biological replicates with relative SEM. (**C**) Representation of the HP1043 consensus sequence positioning in P_{fldA} and P_{rpoD}.

To complete the study of the regulatory activity we moved to bidirectional promoters. To do so, we devised an additional system that utilizes *luxC* and *lacZ* as reporter genes. In this system, the *lacZ* gene was inserted upstream of a bidirectional promoter in the pVAC::Promoter::*luxC*::Km^R vector (Figure 4B). Coincidentally, the extensively validated target P_{hp1227} is indeed a bidirectional promoter. Therefore, we could quickly generate the reporter system *lacZ*::$P_{hp1226/hp1227}$::*luxC* and the two point mutations A1F and T3S, by simply introducing the second reporter gene upstream of the promoter. For transcriptional evaluation, its promoter-less control was generated as previously, using the vector pVAC::*lacZ*::*luxC*::Km^R. By looking at the

schematic representation representing the architecture of the bidirectional promoters, P_{hp1226} and P_{hp1227} (Figure 9A), we notice how the consensus binding sequence falls downstream of the transcriptional start site (TSS) of *hp1226* with the two -10 elements almost overlapping. This configuration suggests a more complex regulation of the expression of the aforementioned genes. The qRT-PCR analysis of *lacZ* indicated that HP1043 was capable of regulating the transcription of both reporter genes, especially during the late exponential phase (Figure 9B). However, further investigation is required to fully understand this phenomenon.

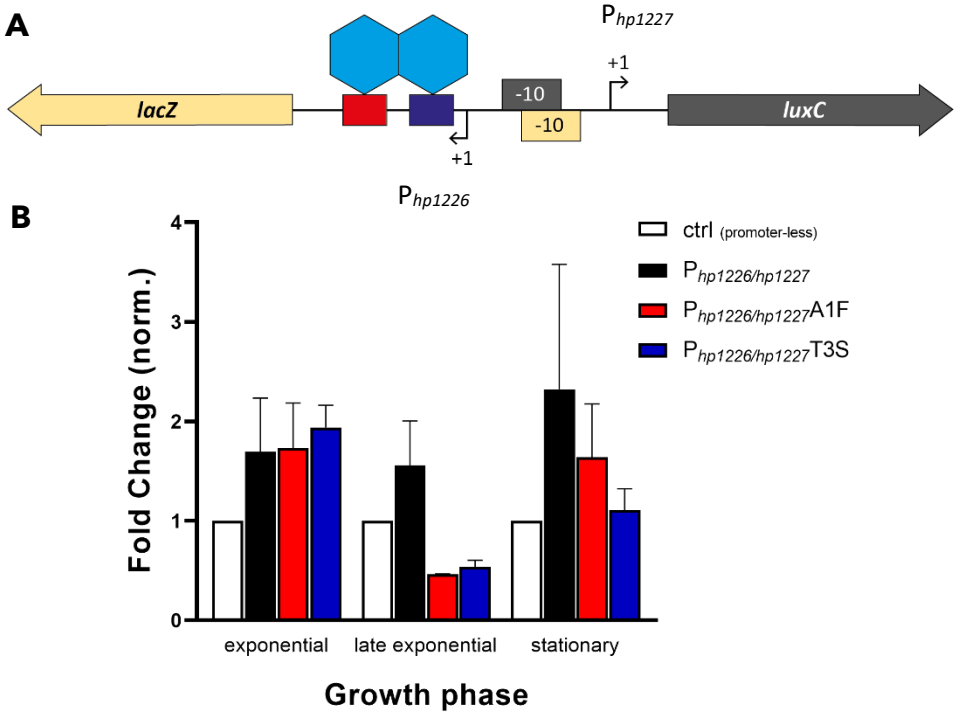

Figure 9: qRT-PCR analysis of the reporter system with *hp1226/hp1227* mutated promoter. (**A**) Schematic representation of the bidirectional promoter of *hp1226/hp1227* in the reporter system. (**B**) *lacZ* transcription levels are indicated as fold change. Data were normalized against the housekeeping *16S* rRNA gene and compared to *lacZ* expression in the promoter-less control strain. *lacZ* transcription levels in G27 *lacZ*::$P_{hp1226/hp1227}$::luxC::Km^R (in black), G27 *lacZ*::$P_{hp1226/hp1227}$A1F::*luxC*::Km^R (red), and G27 *lacZ*::$P_{hp1226/hp1227}$T3S::*luxC*::Km^R (blue) are compared to the control G27 *lacZ*::*luxC*::Km^R (white), in three different growth phase. The graphs represent mean data obtained from technical duplicates of three biological replicates with relative SEM.

At this point, EMSAs were employed to confirm the alteration of HP1043 affinity following point mutation of the consensus binding sequence of target promoters.

We tested and confirmed the *in vitro* affinity of recombinant HP1043 to its wild type promoters, P_{hp1227} and P_{rpoD}. The EMSA analyses exhibited a concentration-dependent reduction in unbound DNA due to target-specific HP1043 binding (Figure 10). A slight smear of the non-specific probe was observed at the highest protein concentration tested.

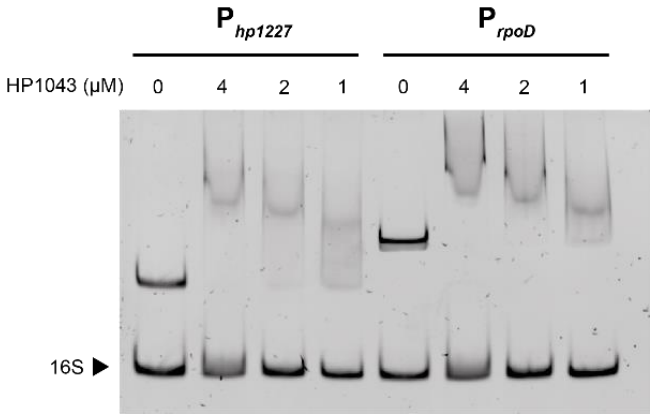

Figure 10: Titration of the two specific DNA probes with recombinant HP1043. All samples contained two DNA probes, one specific on top (P_{hp1227} or P_{rpoD}) and a non-specific on the bottom (16S rRNA gene). HP1043 concentrations used for each reaction are 0, 4, 2, 1 μM. EMSA analysis show a decrease in free probe ((P_{hp1227} and P_{ropD}) in response to decreasing amounts of HP1043 protein, indicative of the formation of specific protein–DNA complexes represented by a shifted band and a smear. The smear represents protein–DNA complexes dissociating during electrophoresis.

Then, EMSA performed for the three promoters (P_{hp1227}, P_{rpoD}, P_{fldA}) wild type and mutant variants (A1F and T3S) showed outcomes consistent with what was observed *in vivo* through qRT-PCR. Lower protein concentrations were employed to assess subtle effects on the DNA-binding affinity generated by the point mutations in the consensus sequence. The point mutations on the P_{hp1227} consensus sequence had a visible impact in decreasing the DNA-binding affinity of HP1043 for its target, as demonstrated earlier by the changes in the transcription level of *luxC* (Figure 11A). In the case of P_{rpoD}, an increase of the unbound DNA was less detectable than P_{hp1227} and expectations based on *in vivo* analysis (Figure 11C). Nonetheless, it became more evident at higher protein concentrations. Lastly, EMSAs conducted on P_{fldA} did not detect appreciable changes in HP1043's binding affinity due to point mutations, even when higher protein concentrations were employed (Figure 11B). All these

findings depicted the possible issues in comparing *in vitro* and *in vivo* data. However, EMSA outcomes further enhance our comprehensive understanding of the interactions between HP1043 and its targets.

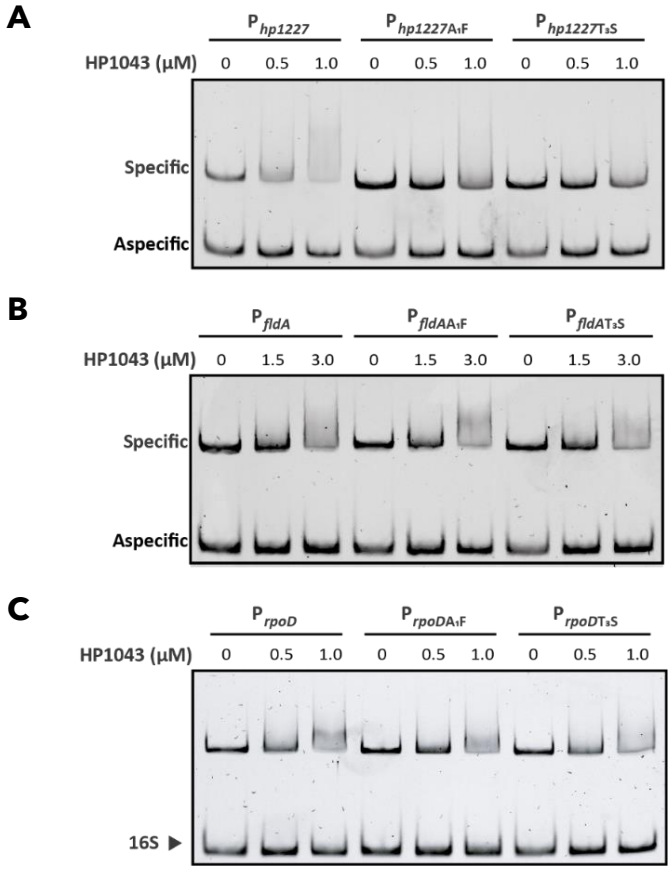

Figure 11: EMSAs of promoter probes containing mutated consensus sequence: All samples contained two DNA probes, one specific on top (P_{hp1227}, P_{rpoD}, or P_{fldA} wild type and their two mutants A1F and T3S) and a non-specific on the bottom (16S rRNA gene). HP1043 concentrations used for each reaction are 0, 0.5, 1, μM for P_{hp1227} and P_{rpoD} probes (**A**, **C**) or 0, 0.5, 1, μM for P_{fldA} probes (**B**).

4.2. Molecular Dynamics simulation leading to HP1043 ligands

As mentioned earlier, the targeting of TRs, such as HP1043, has the potential to be a promising therapeutic strategy for multi-drug resistant bacteria. By inhibiting their biological activity, the downstream effect can be disruptive for the bacterial cell, and hence very promising in treating bacterial infections. In a prior investigation, we examined the ZINC15 18k molecules data bank to find approved and de-risked drugs that bind to the transcription factor HP1043 and reduce its affinity for DNA.

The systematic approach involved the docking of these small molecules to the dimeric conformation of HP1043 in both DNA-bound and unbound states, generating calculated binding energies in agreement with similar studies[74].

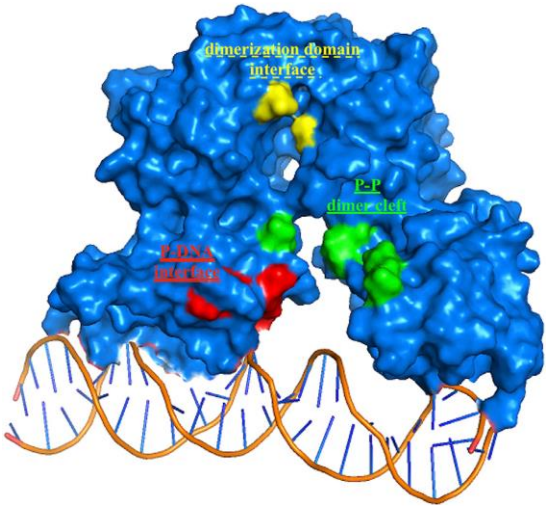

Figure 12: HP1043 binding sites. Residues belonging to the three principal binding sites, in green residues at the dimer cleft, in yellow residues at the dimerization domains interface, and in red residues at the A chain–DNA interface. Adapted from Antoniciello et al., 2022.

The HTVS yielded an initial set of 155 ligands, accounting for 161 distinct binding poses, by considering their predicted binding affinities in the fM and pM range. These ligands were subsequently subjected to a re-docking process and ligands displaying nM or lower binding affinities with a cluster numerosity exceeding 100 units were considered. Among the HTVS molecules, we rejected the compounds that were either unavailable for purchase or prohibitively expensive, as well as ligands that exclusively bound to the DNA molecule. A subset of 13 compounds was chosen for further evaluation through MMGBSA molecular dynamics method. The simulations were carried out in the same complex conformation as the docking results. Eleven of these complexes involved HP1043 bound to DNA, while the remaining six pertained to the unbound form of HP1043 dimer. These selected molecules provided a representation of various binding sites, including the dimer cleft, the interface between the two chains, and a site with lower specificity at the protein-DNA interface (Figure 12). Although the molecular dynamics stability

analysis found that all complexes reached equilibrium during the simulations, two complexes demonstrated ligand expulsion during simulation, indicating a lower affinity for the HP1043_DNA system despite their negative binding energy. Additionally, several complexes showed greater affinity for the DNA molecule than the transcription factor, suggesting low specificity for HP1043. It is noteworthy that a ligand-induced partial unfolding of the C-terminal domain of the monomer and increased DNA bending, whereas other compounds caused movement of the C-terminal domains resulting in mutual rotation and reduced distance between them. By analysing the residues' flexibility in DNA-free complexes, it was noted that the DNA-binding domain residues displayed increased flexibility, while residues situated in the domain interface with the dimerization domain demonstrated reduced flexibility. In investigating the interactions between HP1043 and DNA and their inhibition due to the presence of a ligand, Electrophoretic Mobility Shift Assay (EMSA) proved once again to be a versatile and sensitive *in vitro* tool. A concentration of 4 μM of the HP1043 monomer was chosen as it has shown a binding condition that is not completely saturated. Ligands identified through prior molecular docking and dynamics simulations, which were bound to DNA molecules, were deliberately excluded to avoid non-specific interactions. The study evaluated the inhibitory properties of seven selected ligands, namely plerixafor, tetraethylenepentamine (or TEPA), trientine, ribociclib, dihydroergotoxine, oxcarbazepine, and temoporfin, through EMSA (Figure 13). The test aimed to determine whether the protein-promoter complex formation was hindered by the dynamic interactions between the ligands and HP1043. The extent of the inhibitory effect was quantified based on the relative amount of the free DNA band. Hence, the ligand interference with the specific shift of P_{hp1227} can be correlated in some measure to a potential inhibition of HP1043 activity. The results revealed that temoporfin exhibited a pronounced inhibitory effect at the lowest concentration, i.e., 50 μM, corresponding to a mole monomeric-HP1043 to ligand ratio of 1:12, and displayed a significant reduction in mobility shift of the specific DNA probe at higher concentrations (Figure 13C). Trientine and TEPA also demonstrated notable reductions in DNA-binding activity of HP1043, albeit with faint bands corresponding

to bound promoter DNA still detected in EMSA (Figure 13A, B). Nevertheless, all three ligands exhibited the ability to restore the electrophoretic mobility of free P_{hp1227} in a concentration-dependent manner.

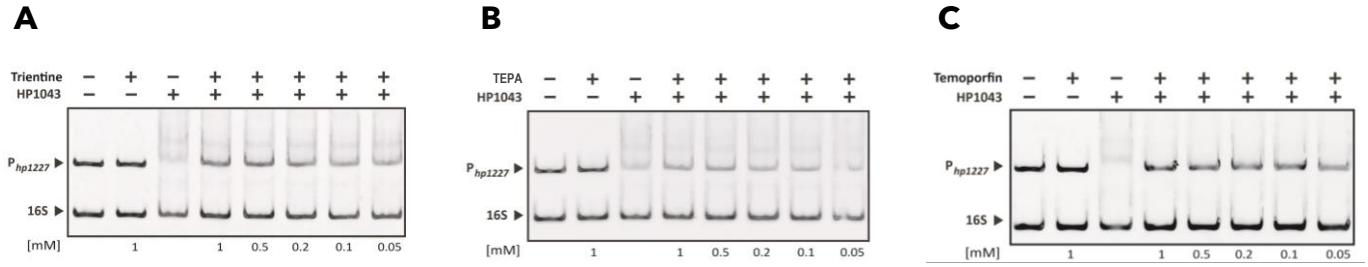

Figure 13: Inhibition of HP1043 Binding to P_{hp1227} by three screened ligands: The figure illustrates the results of EMSA experiments where the recombinant HP1043 protein was incubated with a specific probe (P_{hp1227}) and underneath a non-specific probe (16S rRNA gene), in the presence of decreasing concentrations (1 mM to 50 µM) of the three ligands, trientine (**A**), tetraethylenepentamine (or TEPA) (**B**), and temoporfin (**C**) . Negative control reactions were loaded, including the addition of equivalent volumes of solvent (H_2O and DMSO), and controls to rule out ligand-induced mobility shift in DNA probes. The inhibitory effect on HP1043 binding was quantified based on the optical density of the free DNA band.

On the other hand, four ligands did not display a substantial reduction in the DNA-protein complex under the experimental conditions (data not shown). Starting from the EMSA results, the three compounds that effectively inhibited DNA-binding were subsequently tested on two bacterial strains (G27 and the well-known 26695, for comparison) to establish the minimal inhibitory concentration (MIC) and minimal bactericidal concentration (MBC) (Table 5), and later the evaluation of potential antimicrobial synergies was investigated by checkerboard assay (G27 strain reported only, Table 6). The antimicrobial activity of the promising ligands was related to 2 available antibiotics used to eradicate *H. pylori* infections, levofloxacin and ciprofloxacin. Although the MIC and MBC are higher when compared to the antibiotic, the overall antimicrobial activities are comparable to those reported in the literature for other compounds targeting HP1043[55]. In addition, temoporfin exhibited what seems to be promising synergistic interactions with the two antibiotics, while the TEPA demonstrated additive activity. These results indicate that these compounds have the potential to be valuable candidates for further investigation as re-purposed drugs against *H. pylori* infections.

Table 5: Minimal inhibitory and bactericidal concentration (in brackets) values, expressed in μg/mL, for three screened ligands and two fluoroquinolone class antibiotics. *H. pylori* G27 and *H. pylori* 26695 strains were used to perform the antimicrobial assays.

	Helicobacter pylori strains	
	G27	26695
Compounds	MIC (MBC) [μg/mL]	MIC (MBC) [μg/mL]
TRIENTINE	128 (256)	128 (128)
TEPA	128 (128)	64 (64)
TEMOPORFIN	32 (32)	32 (32)
LEVOFLOXACIN	1 (2)	0.5 (1)
CIPROFLOXACIN	2 (2)	1 (2)

Table 6: Interaction of HP1043 ligands with antibiotics in *H. pylori* G27. The fractional inhibitory concentration (FIC) index could be calculated as: FIC_A (MIC_A in the presence of B/MIC_A alone) + FIC_B (MIC_B in the presence of A/MIC_B alone). According to the FIC index value, the interaction between two compounds against a particular bacterial strain can be classified as: synergy (FIC index ≤ 0.5), additive (0.5 < FIC index ≤ 1), no interaction or neutral (1< FIC index ≤4), and antagonism (FIC index > 4).

Strain	Combination tested	$FIC_{antibiotic}$	FIC_{ligand}	FIC index	Interaction
H. pylori G27	LEVO + TRIENTINE	0.75	0.25	1	additive
	LEVO + TEPA	0.5	0.125	0.625	additive
	LEVO + Temoporfin	0.25	0.0625	0.3125	synergy
	CIP + TRIENTINE	0.5	0.75	1.25	neutral
	CIP + TEPA	0.5	0.5	1	additive
	CIP + Temoporfin	0.25	0.125	0.375	synergy

4.3. Co-crystals

In recent years, the exploration of innovative strategies in antimicrobial drug discovery has brought research towards crystal engineering. Co-crystallization is a versatile tool that offers promising routes for synthesizing new materials and enhancing the properties of existing active compounds. Our study involved the co-crystallization of two fluoroquinolone antibiotics, levofloxacin (LEVO) and ciprofloxacin (CIP), with three flavonoids: quercetin (QUE), myricetin (MYR), and hesperetin (HES) (Table 7). The fluoroquinolones employed in this study were

chosen based on their reported clinical interest as effective drugs against *H. pylori*[99-101]. These flavonoids, derived from various natural sources, have garnered attention for their potential therapeutic benefits, including antimicrobial properties. Recent studies suggest the capacity of some flavonoids to inhibit HP1043 DNA-binding, leading to antimicrobial activity against *H. pylori* [14,55]. Therefore, our work begins with this basis to introduce a unique multitarget approach. This involves the synthesis of co-crystals of an antibiotic and a flavonoid and represents the first instance of enhancing antibiotic efficacy by targeting a bacterial TR that is necessary for bacterial pathogenicity.

Table 7: Molecular structures of the fluoroquinolones and flavonoids used in this work.

FLUOROQUINOLONES		**FLAVONOIDS**		
LEVOFLOXACIN	CIPROFLOXACIN	QUERCETIN	MYRICETIN	HESPERETIN
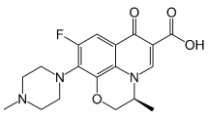	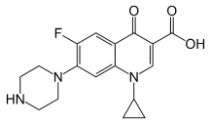	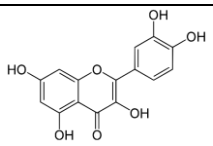	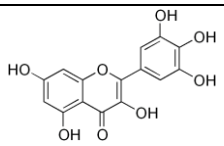	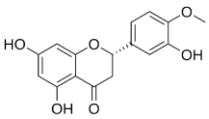

All the co-crystals were obtained using a 1:1 or 2:1 stoichiometry between the fluoroquinolone and the flavonoid, respectively the co-crystal suspensions of levofloxacin and quercetin (LEV·QUE), levofloxacin and hesperetin (2LEV·HES), and ciprofloxacin and quercetin (CIP·QUE) contained respectively 50%, 33%, and 50% fewer antibiotics, in terms of moles of levofloxacin or ciprofloxacin. After conducting a comprehensive physical-chemical analysis of the synthesized co-crystals, we proceeded with evaluating their antimicrobial activity via MIC and MBC. The results listed in the table highlight in particular that tested flavonoids alone exhibit high MIC against both *H. pylori* strains, G27 and 26695 (Table 8). Nonetheless, these first tests showed promising antimicrobial activities by co-crystals of antibiotics and flavonoids, showing that the combination of the two classes can lead to advantages in the application of the antimicrobial therapies. The co-crystals of levofloxacin with hesperetin and quercetin showed the highest potential. The same results were

observed for the physical mixture controls, where equal moles of compounds were used to be compared with the co-crystalline form. An explanation for the results is that antibiotics and flavonoids co-crystallize when they are physically mixed in experimental conditions, obtaining the same antimicrobial effect on bacteria. Overall, we conclude that for *H. pylori*, the combination of flavonoids with an antibiotic capable of forming co-crystals may be a new and advanced approach to reduce the total amount of antibiotic used for treatment while maintaining the same antimicrobial efficacy. This result is in line with the recommendations and guidelines of the WHO and WGO[4] to reduce the use of antibiotics to prevent or at least slow the emergence and spread of antibiotic-resistant pathogenic strains.

Table 8: Minimal inhibitory and bactericidal concentration (in brackets) values for co-crystals, physical mixtures (indicated with a "+"), and single compounds. *H. pylori* G27 and *H. pylori* 26695 strains were used to perform the antimicrobial assays.

	Helicobacter pylori strains	
	G27	26695
Compounds	MIC (MBC) [µg/mL]	MIC (MBC) [µg/mL]
LEV·HES	1 (2)	0.5 (1)
LEV + HES	1 (2)	0.5 (1)
LEV·MYR	4 (8)	2 (4)
LEV + MYR	4 (8)	4 (8)
LEV·QUE	1 (2)	1 (2)
LEV + QUE	1 (2)	1 (2)
LEVOFLOXACIN	1 (2)	0.5 (1)
CIP·QUE	2 (4)	1 (2)
CIP + QUE	2 (4)	2 (2)
CIPROFLOXACIN	2 (2)	1 (2)
HESPERETIN	128 (256)	128 (256)
MYRICETIN	256 (512)	256 (512)
QUERCETIN	512 (512)	256 (512)

4.4. Peptide Nucleic Acid targeting *hp1043*

A class of short antisense oligomers called PNAs has recently emerged because of their attractive antisense activity and high specificity. PNAs can be used for the gene silencing of vital bacterial genes by blocking the translation of the target mRNA. As bacterial uptake is a general challenge for the application of PNAs, they are conjugated to bacterial penetrating peptides (BPP) to enhance the crossing of the lipopolysaccharide layer and both the outer and inner membrane. PNA-BPP conjugates targeting critical bacterial genes have been successfully tested against several pathogens, showing high potential as antisense antimicrobials. The correct design of the PNA complementary sequence and the screening of the most suitable BPP are crucial steps for their use and efficient gene knockdown. To assess the feasibility of such an approach in *H. pylori* as well as the specific targeting of one of its key regulators, we designed and employed antisense PNAs to downregulate the HP1043 protein level in the cell. The molecular antisense mechanism of PNAs in bacteria has never been fully characterized. However, it is believed to rely on the inhibition of the translation through steric hindrance of ribosome assembly on the mRNA. In simpler terms, PNA-induced silencing in bacteria results in repression of translation.

For our third innovative strategy to target HP1043, the PNAs were designed to match *hp1043* mRNA and knock down its expression. This approach could eventually lead to the dysregulation of a cluster of critical genes controlled by HP1043 and hence generate a novel multitargeting approach against *H. pylori*. In addition, the use of PNAs can provide a versatile tool for gaining a deeper understanding of the regulatory mechanisms involving the TR, which is hampered by its vital role in the cell. These PNAs' complementary sequence maps around the RBS and the start codon, with PNAs ranging from 11 to 8 nucleobases (Figure 14). It has been experimentally demonstrated that 8-mer to 11-mer PNAs are the most effective against *E.coli*, with the optimal length being 10 nucleobases. The explanation for this optimum was proposed by Goltermann and coworkers (2019), showing how longer molecules have reduced uptake properties while shorter ones have less PNA:RNA

duplex stability. To achieve an efficient internalization by *H. pylori*, two different BPPs, H-$(KFF)_3$K-eg1 and H-$(R\text{-}X)_6$-X, were conjugated to PNAs and tested for uptake efficiency. These BPPs contain cationic and hydrophobic amino acids, namely lysine, d-arginine, and phenylalanine.

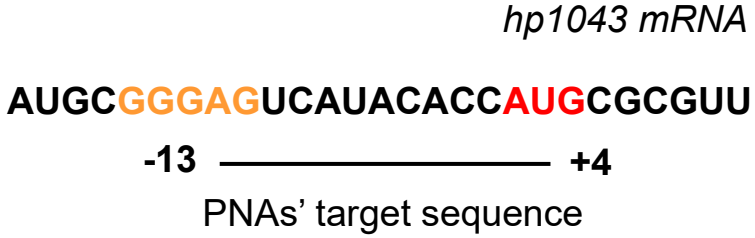

Figure 14: Schematic representation of the PNAs' target region (indicated by a line) of *hp1043*. The start codon is displayed in red, with the A counting as +1, and in orange the RBS (from -10 to -14)

We began our investigation by checking the gene knockdown effect on *in vitro* models that exploit the PURExpress® kit to detect GFP fluorescence and chemiluminescence. The plasmid carrying the target RBS and the first 221 nucleotides of *hp1043* fused in frame with a mutated GFP (Figure 15A) was mixed with the kit solutions and increasing amounts of BPP-PNA conjugates. Since the kit is optimized for high yields of proteins, we did not expect a significant reduction of the expression when plasmid was used as a template. Figure 15B shows the relative fluorescence of the fused GFP in the presence of matching PNAs compared to the non-treated sample. It is interesting to note that the reduction of the signal is concentration-dependent, achieving an overall 50% reduction of the signal 5 μM, the highest concentration of conjugates tested. While, the mismatches did not produce an effect on the fluorescence intensity, with values that range within the not-treated one. The same analysis was performed specifically on two conjugates (11-mer and 8-mer) using both plasmid and mRNA carrying full-length *hp1043* gene and evaluating protein expression through immunoblotting. Once again, the gene silencing activity of the PNAs *in vitro* was demonstrated as well as a correlation between the length of the antisense oligomer and the stability of the PNA-RNA duplex. The first results confirmed the actual *hp1043* gene knockdown capacity of

the BPP-PNA conjugates *in vitro* with different conditions that somewhat mimic the gene expression in the bacterial cell. The western blot analysis exhibited the gene silencing capacity of PNAs *in vitro* along with the correlation between the length of the antisense oligomer and its inhibitory effect. The 11-mer displayed a greater reduction in translation at lower conjugate:plasmid ratios (250:1) compared to the 8-mer (Figure 15C), whereas both oligomers exhibited a similar impact when using RNA, even at the lowest conjugate:mRNA ratio tested (10:1) (Figure 15D). The length of tested PNAs did not show to have a significant impact on the silencing effect of the conjugates when the plasmid was used as a template. However, a difference appeared when using mRNA for the reactions, suggesting the importance of the quantity of template material in the *in vitro* reactions.

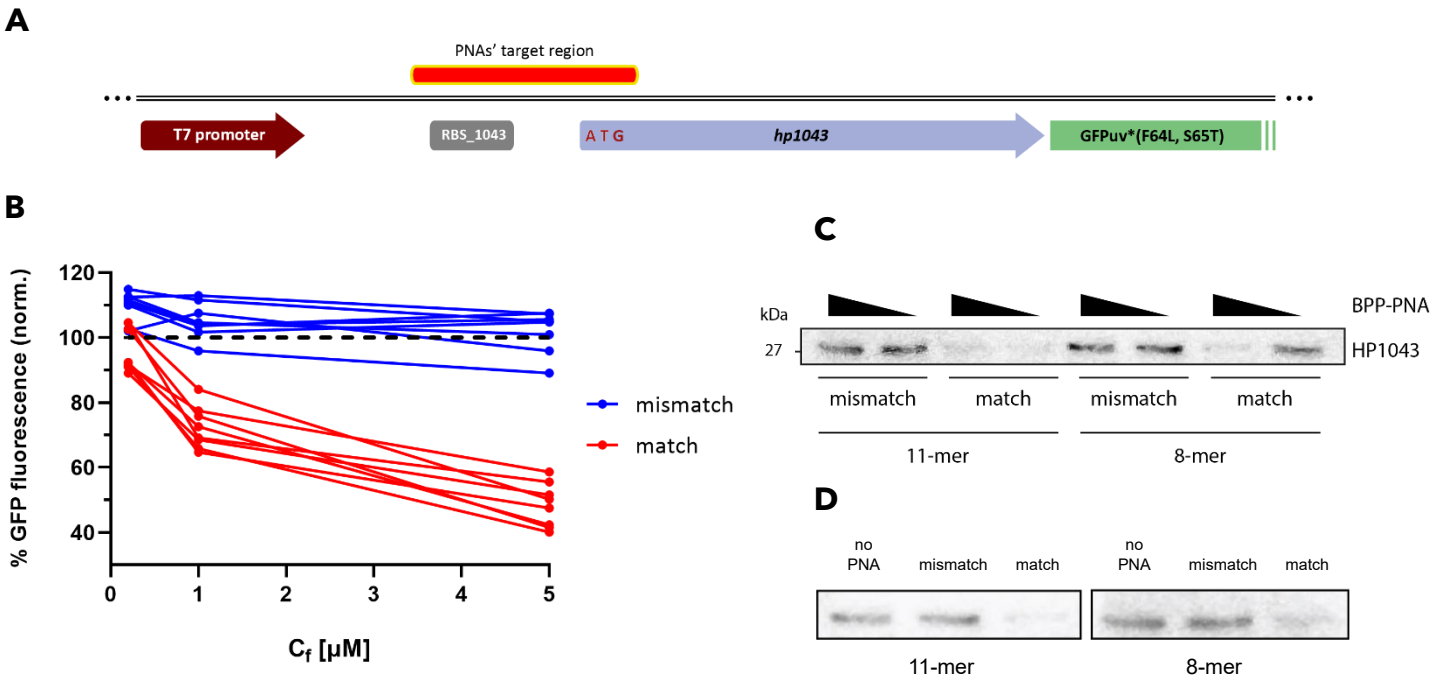

Figure 15: *in vitro* translation reactions. (**A**) Schematic representation of the transcribed section of the plasmid (p411::P_{T7}::RBS_{hp1043}::*hp1043(221)*::GFPuv*) carrying the T7 promoter, the *hp1043* RBS, the PNA-targeted region (red) and the HP1043 (221nt)-GFPuv fused protein. (**B**) Percentage of GFPuv-produced fluorescence detected for *in vitro* translation reactions in the presence of variable concentrations (0.2, 1, 5 μM) of BPP-PNA conjugates and normalized on the negative control, in absence of conjugates, displayed as a dotted black line. Match BPP-PNA conjugates are reported in red while mismatch BPP-PNA conjugates are reported in blue. *In vitro* translation reactions using the p411::P_{T7}::RBS_{hp1043}:: *hp1043* vector (**C**) or its mRNA (**D**) as template, in the presence of variable concentrations (1 and 5 μM) of BPP-PNA conjugates. Specifically, the 11-mers 5971 (match) and 5973 (mismatch) and the 8-mers 6255 (match) and 6256 (mismatch). As control, an equal volume of water was added ("no PNA"). Western blotting was performed for detection of HP1043 (~27 kDa) by using an anti-HP1043 antibody.

The second aspect that needed to be addressed was the uptake efficiency of PNAs in the case of *H. pylori*. To do so, non-specific BPP-PNA conjugates (5509, 6278) were linked to a fluorescence probe (BODIPY FL) and incubated with bacteria for 1h, following what previous studies indicate as sufficient time for near 100% uptake in *E. coli*. Two BPPs (the lysine and arginine-rich peptides) were tested at two different concentrations, 16 μM and 8 μM (Figure 16). The images qualitatively show that both conjugates were able to penetrate the membranes and reach the PNA target, i.e., *hp1043* mRNA, at both concentrations. Interestingly, after only 1h of incubation, the $(KFF)_3K$-PNA conjugate (6278) seemed to have affected the shape of *H. pylori*, making bacterial cells shift from a curved rod profile to a coccus-like appearance (Figure 16B, D). It is also noticeable that the BPP-PNA conjugates were not equally distributed throughout the bacterial cells, as single spots, plausibly inside the cell, were detected with higher resolution (Figure 16E). This phenomenon could be ascribed to aggregation between conjugates once internalized or to accumulation in vesicles, which could ultimately lead to an overall diminished gene knockdown effect, and thus prospected lower antimicrobial activity. To better evaluate BPP-PNA conjugates' uptake efficiency, we performed the same experiment on both *H. pylori* and *E. coli*, which has been extensively validated by the research group led by P.E. Nielsen[66,69]. A major difference in fluorescence intensity between these two bacterial species was observed, presumably indicating a distinct internalization efficiency of the conjugates investigated (Figure 16F). According to the microscope imaging performed, it appears that both PNAs conjugated to the $(KFF)_3K$ and $(dR\text{-}eg1)_4$ peptides exhibit no specificity towards *H. pylori* and lower uptake in comparison to an established model species, i.e. *E. coli*.

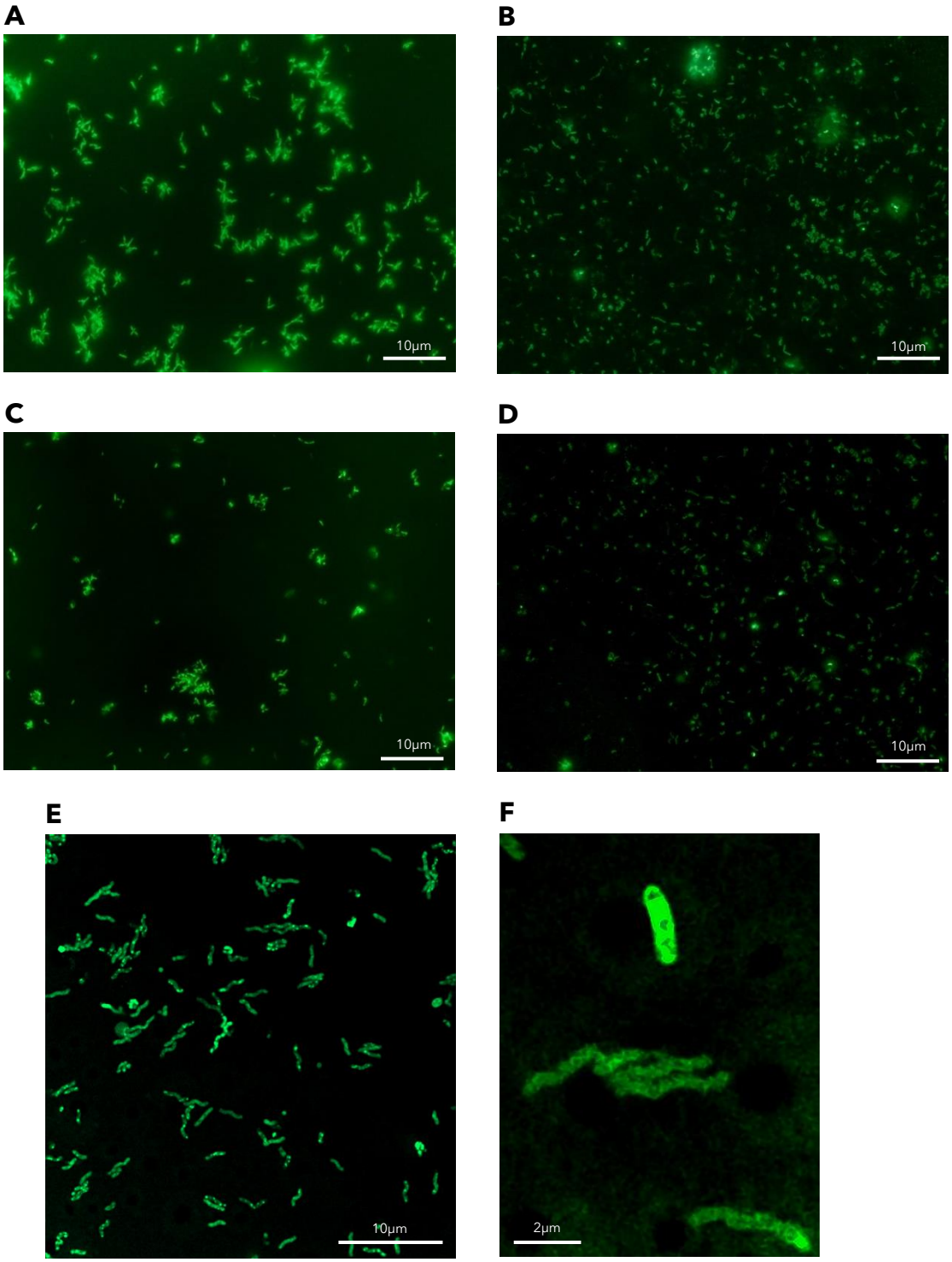

Figure 16: Microscope images of *H. pylori* G27 treated with two BODIPY_FL-labelled BBP-PNAs, 5509 (**A**, **C**, **E**) and 6278 (**B**, **D**) for 1h (green channel: excitation at 488 nm). Specifically, the G27 strain was treated with 16 µM (**A**,**E**) and 8 µM (**C**) of 5509, carrying the H-(R-eg1-R)$_4$ peptide, and 16 µM (**B**) and 8 µM (**D**) of 6278, carrying the H-(KFF)$_3$K peptide. (**F**) Close look of *H. pylori* G27 (faint-green elongate bacteria) and *E. coli* DH5α (intense-green bacterium on top) treated with 8 µM of 5509.

Next, to confirm the gene silencing capacity of PNAs on *H. pylori* cells, we designed and employed anti-*ftsZ* BPP-PNA conjugates. FtsZ is a tubulin-like protein that is essential for bacterial cytokinesis: it forms a Z-ring at the mid-cell which serves as a scaffold for the assembly of the divisome, facilitating cell division. When the expression of *ftsZ* is inhibited, the Z-ring cannot form, leading to a disruption in the cell division process. Bacteria with inhibited FtsZ expression often exhibit elongated or filamentous morphologies due to the inability to complete cell division. This approach enables straightforward microscopy-based confirmation of gene knockdown efficacy. As expected, the treatment of *H. pylori* with specific anti-*ftsZ* BPP-PNA conjugates resulted in prolonged chains of undivided bacterial cells (Figure 17A). When comparing with the untreated bacteria and, more significantly, with the bacteria exposed to high concentrations of mismatch BPP-PNA conjugate, the variation in unit shape is striking. For a more objective and quantitative assessment, the length of 50 cells/units in each treatment was measured, and the results are reported in Figure 17B. The mean value of the measured objects shows a significant increase (from 3.5 to 9.3 μm) for bacteria exposed with the matching PNA, with a more widely distributed population and cases out of scale (>25 μm). The microscope images together with the statistical analysis of the bacterial length corroborate the potential of antisense agents, such as PNAs. The phenotypic differentiation observed was concentration-dependent and the high amounts of compound needed suggest that the BPP conjugated to the effective PNA could not ensure efficient uptake in *H. pylori* without using high concentrations.

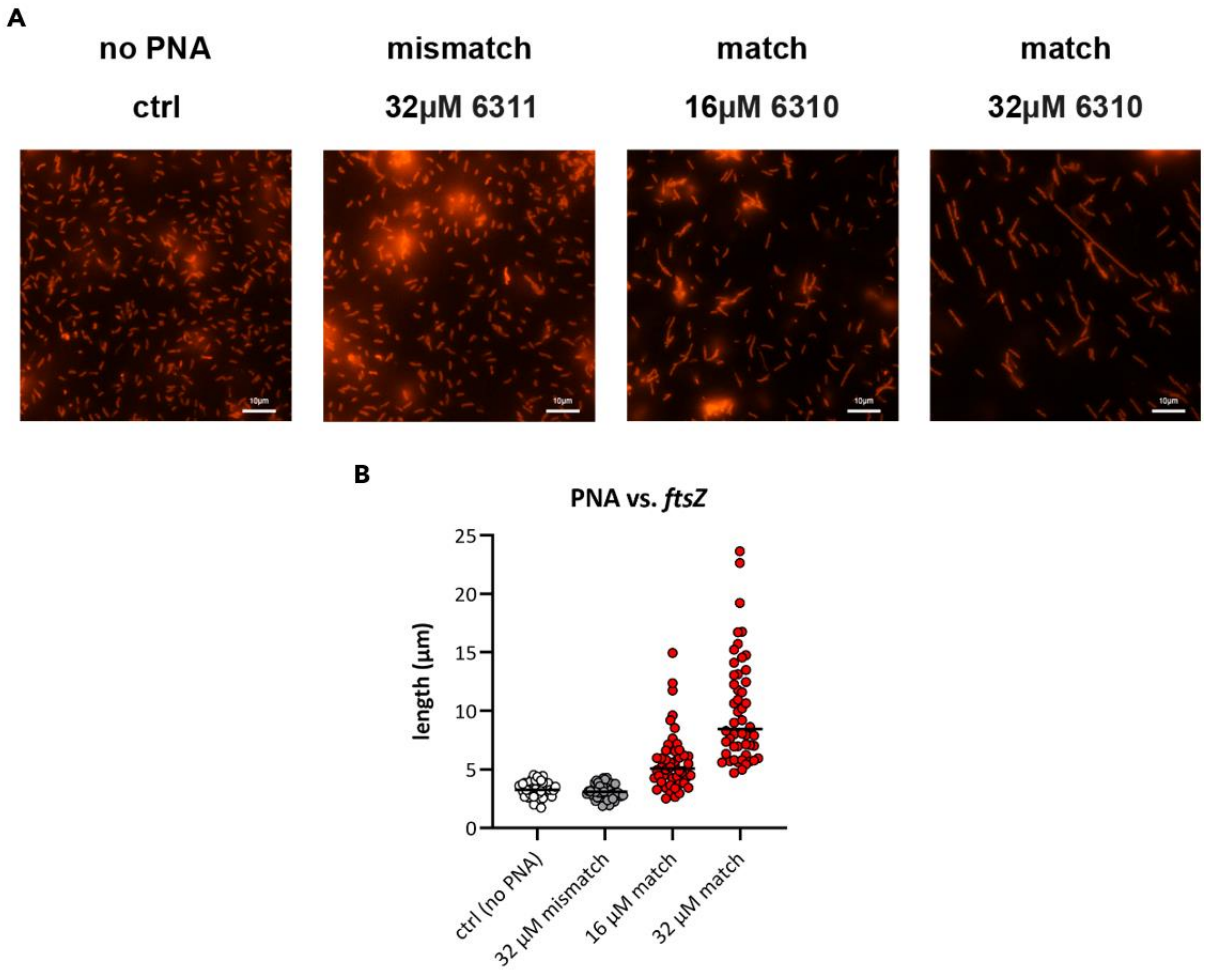

Figure 17: (**A**) Microscope images of *H. pylori* treated with 32 and 16 µM of anti-*ftsZ* BPP-PNA conjugate (6310) and 32 µM of its relative mismatch (6311). As control, an equal volume of water was added ("no PNA"). (**B**) The length of 50 bacterial cells/units per image was quantified using ImageJ tools and shown in a scatter plot. Medians are indicated with a black line and measurements in white circles for the control, grey for the mismatch, and red for the match.

Finally, the antibacterial efficacy of the compounds was assessed. MICs were measured against three strains of *H. pylori* (G27, and other two well-established *H. pylori* strains for comparison, 26695 and P12) according to the standard method illustrated by Nielsen and Goltermann (Table 9). The target position, BPP, and MIC values for each conjugate are summarized in the table below. Notably, PNA 6124, a 10-mer targeting the region surrounding the AUG, gave the lowest MIC values, namely 8 µM for G27 and 4 µM for the other two strains. Compared to previous studies that evaluated the antisense activity of PNA against different bacterial species and targets, the minimum inhibitory concentrations achieved against *H.*

pylori were relatively higher. However, it is worth noting that the growth was not affected in the presence of the analogous mismatch PNA (6126), with a MIC above the detectable range. Hence, the antibacterial activity can be attributed to the antisense mechanism of action. This agrees with previous research that identified the optimal length as 10 nucleobases. Various other PNAs with nucleobases ranging from 8 to 11 and carrying different BPP, even split peptides on both extremities, yielded varied and more variable results. Some exhibited slight antimicrobial activity varying between strains, while others demonstrated lower antisense (match/mismatch) specificity. Moreover, these observations indicate that the *hp1043* sequence target is conserved among tested strains, further indicating the potential value of HP1043 as a target. Finally, altering the BPP form from the lysine-rich to the d-arginine-rich peptide did not appear to have any significant impact on the MIC.

Table 9: PNAs and MIC values.

			H. pylori strains		
			G27	26695	P12
No.	BPP	Target Position (ref. start codon)	MIC [μM]	MIC [μM]	MIC [μM]
5970	H-$(KFF)_3$K	from -7 to +4	16	8	16
5972	H-$(KFF)_3$K	from -7 to +4	32	16	32
5971	H-$(dR\text{-}eg1\text{-}dR)_4$	from -7 to +4	32	16	16
5973	H-$(dR\text{-}eg1\text{-}dR)_4$	from -7 to +4	> 32	> 32	> 32
6124	H-$(dR\text{-}eg1)_6$	from -6 to +4	8	4	4
6126	H-$(dR\text{-}eg1)_6$	from -6 to +4	> 32	> 32	> 32
6125	H-$(dR\text{-}eg1)_6$	from -5 to +4	16	8	16
6127	H-$(dR\text{-}eg1)_6$	from -5 to +4	32	> 32	> 32
6255	H-$(dR\text{-}eg1)_6$	from -5 to +3	16	16	16
6256	H-$(dR\text{-}eg1)_6$	from -5 to +3	32	> 32	32
6265	H-$(dR\text{-}eg1)_6$	from -13 to -5	16	8	8
6266	H-$(dR\text{-}eg1)_6$	from -13 to -5	> 32	> 32	32
6267	H-$(dR\text{-}eg1)_6$ and $(eg1\text{-}dR)_3$-NH_2	from -5 to +3	16	8	16
6268	H-$(dR\text{-}eg1)_6$ and $(eg1\text{-}dR)_3$-NH_2	from -5 to +3	32	> 32	32
6312	H-$(KFF)_3$K	from -3 to +5	32	16	16
6313	H-$(KFF)_3$K	from -3 to +5	> 32	> 32	32

To validate the PNA antisense target specificity, hence confirming that the growth inhibition was due to lower HP1043 expression rather than due to cationic peptides' antimicrobial effect, western blotting followed the MIC assay on the most promising match-mismatch couple (6124-6126) was carried out (Figure 18). Bacterial samples exposed to 1 x MIC to 1/16 of MIC of the match were compared to the higher mismatch concentration and the untreated bacteria. The analysis demonstrated a

90% decline in HP1043 levels when exposed to MIC (16 μM in this case) (Figure 18A, B), while no significant difference was apparent between ½ MIC (8 μM) and ¼ MIC (4 μM), resulting in a reduction of approximately 55% compared to the protein level observed in the absence of BPP-PNA conjugate (Figure 18B). Then, a concentration of 1 μM resulted in the loss of gene knockdown, with normal protein expression restored. Moreover, the mismatch not only did not decrease the amount of protein expressed by the cells but also produced a slight increase as it can be deduced by the higher intensity of the signal. This is noteworthy as it smoothly aligns with the results of the in vitro translation reactions.

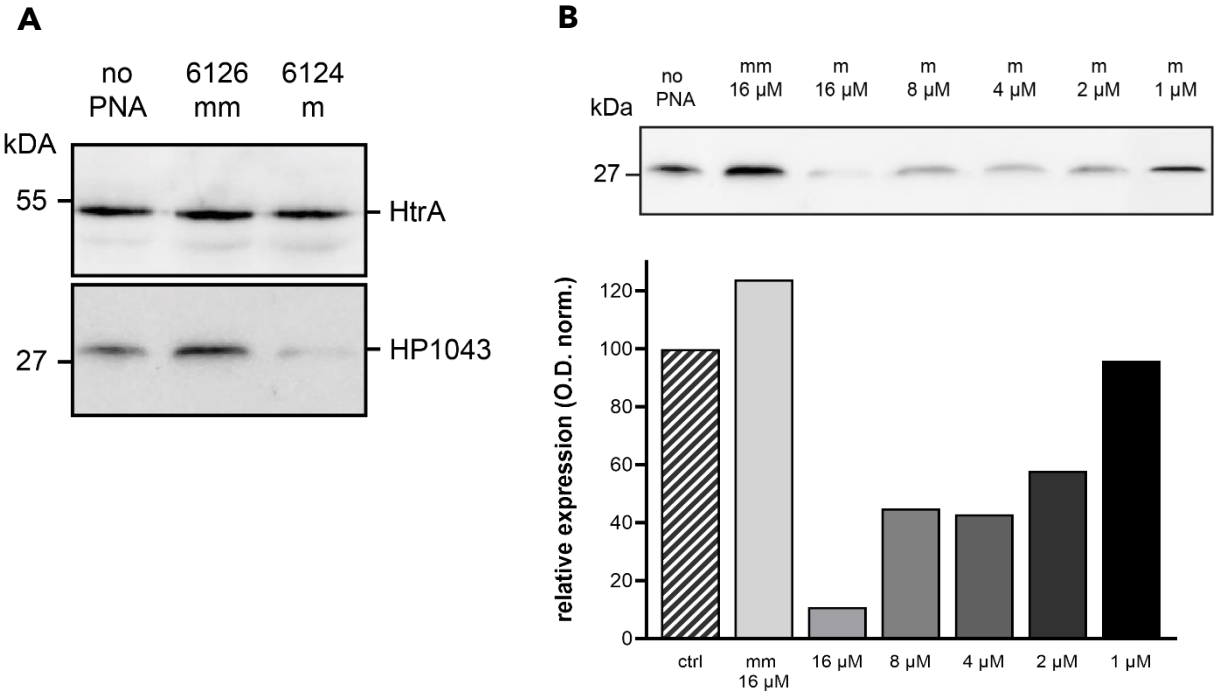

Figure 18: The antisense BPP-PNA conjugate 6124 targeting *hp1043* inhibits translation of its target *in vivo*. (**A**) MIC samples of *H. pylori* G27 treated with 16 μM of the match (m) 6124, 16 μM of the mismatch (mm) 6126, and the control not-treated (no PNA), where an equal volume of water was added. HtrA (~54 kDa) was chosen as a loading control and detected through an anti-HtrA antibody. (**B**) Titration of the H-(dR-eg1)$_6$-10-mer 6124 ranging from 2 x MIC to 1/8 MIC, was analysed through western blot and compared to the mismatch 6126 and the control not-treated. HP1043 (~27 kDa) signal intensity was quantified using ImageJ and protein expression is shown relative to the not-treated control. The experiment was performed once.

For our final analysis on anti-*hp1043* PNAs, we examined the impact of the decreased protein levels observed on the morphology of *H. pylori*. To rule out any

variability in phenotype caused by late growth state-induced stress, we exposed the bacteria to 16 μM of the most promising conjugate 6124 (match) and its mismatch (6126) for 12 hours. As shown in the images, the fitness of bacteria was affected by the match, as deducible by the overall lower numbers of bacterial cells, and coccoid-shaped more curved bacteria were detected for both treated samples (Figure 19). A heterogeneous population of coccus-like and rod-like cells can be seen for all samples, yet a slight shift in morphology towards the typical one of *H. pylori* G27 is appreciable for not-treated and in minimal part for the mismatch. However, we observed no significant correlation between the lower level of protein expression and the differences in phenotype, and thus HP1043 knockdown cannot be considered to be a causal factor so far.

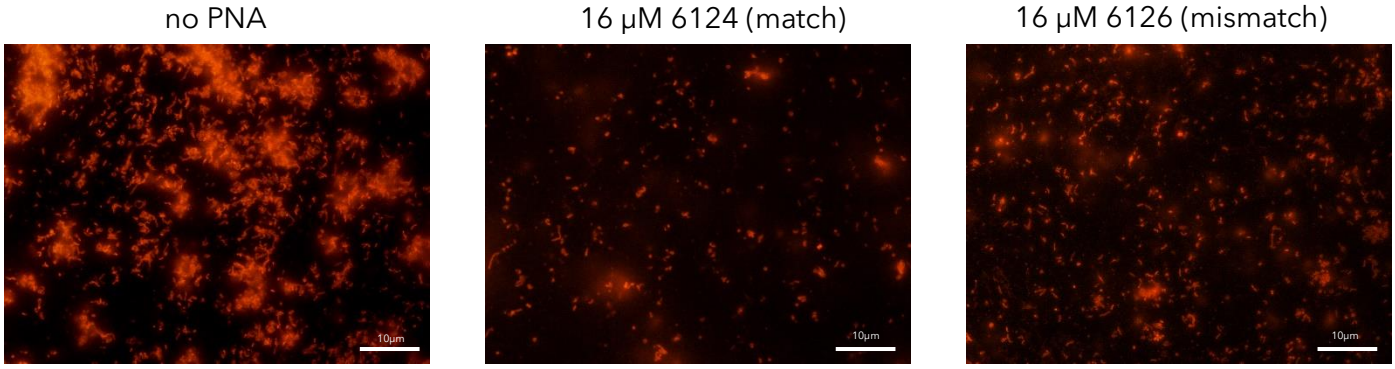

Figure 19: Microscope images of *H. pylori* treated with 16 μM of anti-*hp1043* BPP-PNA conjugate (6124) and 16 μM of its relative mismatch (6126). As control, an equal volume of water was added ("no PNA").

5. DISCUSSION

Antimicrobial resistance (AMR) is an escalating and worrying issue in modern times. The repeated and uncontrolled use of antibiotics in clinical practice has created a selective pressure that led to the growth and spread of resistant bacteria[102]. Novel approaches have looked at TRs as promising therapeutic targets that could offer a solution to this global health threat. Bacterial TRs are usually cytoplasmic soluble proteins lacking a human counterpart and controlling the expression of a multitude of genes crucial for the pathogenicity and survival of the cell[35,56]. HP1043 can be a promising target candidate for treating *H. pylori* infection because of its involvement in regulating major molecular processes[34]. On the other hand, its central role hampers the study of its regulatory function using conventional approaches. The extensive study detailed herein has gained encouraging insights into the intricate functioning of the TR HP1043. Through a versatile reporter system and a series of *in vivo* and *in vitro* analyses, we have explored deeper into the regulatory mechanisms of such a central player in *H. pylori*. By leveraging the *luxC* as a reporter gene[98], we detected for the first time HP1043's *in vivo* regulatory mechanism on a selection of known targets. Our control (P_{hp1227}), with an extensive *in vitro* validation as a target of HP1043[35,49], has allowed us to test our reporter system and thus confirm the transcriptional activation of *hp1227* by the TR (Figure 5A). This promoter acted as an internal control and a crucial benchmark for assessing the effectiveness of our reporter system on other less explored targets. *fldA*, *tlpB,* and *rpoD* proved to be suitable for investigating their regulation via the reporter system we implemented, giving us an initial understanding of their regulation. To reinforce our findings, we extended our analysis to include *hp1227*, *fldA*, and *rpoD* promoter regions that carry point mutations within the HP1043 consensus sequence, particularly in the first or second hemisite. These mutants were selected based on previous mutagenesis analysis that involved a series of *in vitro* assessments, such as DNase I footprinting and transcription assays[35]. The analyses reported here demonstrated HP1043's involvement in the *in vivo* regulation of the same targets, highlighting once again the critical role of specific nucleotides in both hemisites for HP1043's DNA affinity

(Figure 7, 8). Moreover, the use of point mutations in our reporter system shed some light on a possible correlation between the binding site's location and HP1043-mediated transcriptional regulation. Quantitative RT-PCR analysis uncovered the ambivalent activity of this regulator, which appeared to display both activation and repression of target gene transcription. Indeed, P_{rpoD} wild type showed lower transcriptional levels than the promoter-less strain, while mutations inserted in the consensus sequence led to a partial loss of protein binding and thus a reduced repression of basal transcription (Figure 8). To validate our findings, we harnessed EMSAs versatility to confirm *in vitro* the alteration of HP1043's interaction with target promoters following point mutations in the consensus binding sequence (Figure 11). These analyses largely reflected the trends observed in liquid cultures through qRT-PCR, offering robust validation of our results. Since P_{rpoD} differs from other targets, such as P_{fldA} and P_{hp1227}, having a confirmed HP1043 consensus sequence located adjacent to the -10 sequence, its regulation mechanism presents an intriguing opportunity for investigating the interaction between HP1043 and RNA polymerase. In addition, our reporter system allowed us to expand our study on bidirectional promoters, introducing *lacZ* as the second reporter gene. The qRT-PCR analysis on the bidirectional promoter $P_{hp1226/hp1227}$ indicated that HP1043 could regulate the transcription of both reporter genes (Figure 9). However, further investigation is needed to fully understand this phenomenon. It is crucial to consider the complexities of in vivo conditions when considering the data presented on the HP1043 regulation. As reported for other TRs, different molecular players can be involved in the fine regulation of the transcription and hence a more elaborate regulation should not be excluded[26,52]. These findings also have significant implications for the development of multi-targeting strategies that aim at impeding the HP1043 regulatory machine. In this sense, co-crystallisation and drug repositioning techniques provided innovative and efficient alternatives for novel drug discovery, presumably reducing both cost and time[74,79]. Firstly, a series of co-crystals containing fluoroquinolone antibiotics and flavonoids, bioactive compounds with a reported effect on HP1043 binding affinity[14,55], have been synthesized and characterized successfully. The MIC assay presented herein depicts

co-crystallisation as a potential solution to lowering the amount of antibiotic used in therapy while retaining the same antimicrobial effect. Furthermore, data from co-crystals and physical mixtures inspire further investigation into the mechanisms underlying the interaction between solid-state chemistry and the biological realm. Secondly, three promising candidates, namely temoporfin, tetraethylenepentamine, and trientine, were screened, simulated *in silica* and tested both *in vitro* and *in vivo*. Protein binding analysis revealed different localization for ligand-protein interaction, particularly at the protein-DNA interface and the dimer cleft (Figure 12). Furthermore, the compounds exhibit a clear inhibition pattern on HP1043 binding and subtle but remarkable antimicrobial activity (Table 8, Figure 13). Of particular interest, temoporfin demonstrated promising synergistic interactions with both fluoroquinolones. Such synergy can significantly enhance the overall antimicrobial effect, potentially leading to more effective treatments against *H. pylori* infections (Table 6). The binding capacity observed with these drugs towards HP1043 presents them as potential inhibitors with clinical relevance. The results from the repositioning study and the co-crystallization approach underscore the importance of exploring novel targets, i.e., HP1043. In light of this, antisense antimicrobial agents that can specifically regulate HP1043 protein level draw attention.

Antisense PNAs conjugated with specific BPPs are innovative antibacterial agents that can be designed to target essential bacterial genes[65,67]. They have emerged as a potential game-changer in the fight against antibiotic-resistant bacterial infections due to their molecular mechanism of action combined with the specific gene targeting. Our study presents a methodical investigation of the antisense activity and uptake efficiency of BPP-PNA conjugates targeting HP1043. *In vitro* experiments confirmed that our designed PNAs have the ability to specifically inhibit target translation in a concentration-dependent manner (Figure 15). We then evaluated the efficient uptake of BPP-PNA conjugate and examined the potential variations induced by different BPPs. While uptake was ensured for both BPP (lysine-rich and d-arginine-rich), the distribution of the compounds inside the cells was not

homogenous (Figure 16E). Moreover, the $(KFF)_3K$ peptide conjugated to the non-specific PNA induced a partial modification in *H. pylori* morphology (Figure 16). The marked difference in uptake observed between *H. pylori* and *E. coli* demonstrates a greater intensity of the signal due to a higher quantity of PNA internalised (Figure 16F). While definitive conclusions cannot be drawn at this stage, it is likely that the two uptake efficiencies observed between *H. pylori* and *E. coli* may have been the result of a different membrane permeability that does not exclude the presence of efflux systems promoting the removal of PNAs. This hypothesis is substantiated by prior research in related bacterial systems where efflux pumps, such as SbmA, have been identified as key players in the expulsion of BPP-PNA conjugates[66]. One possible approach proposed in literature is the use of a mixture of PNAs targeting different genes to achieve a greater and more coordinated effect on bacterial viability[67,68]. Successively, we verified the knockdown effect through the use of a BPP-PNA conjugate that targets *ftsZ* (Figure 17). The phenotypic changes observed are the result of arrested cell division and demonstrate the compound's specific antisense activity against *H. pylori*. However, the high concentration needed to induce such changes can be another sign of the reduced uptake seen through fluorescence PNAs. Furthermore, inhibition of FtsZ expression in bacteria can result in a non-dividing cell population causing improper separation of cellular contents and eventually leading to cell death or a state of dormancy[103,104]. Anti-*ftsZ* PNAs have been explored with success in *Acinetobacter baumannii*, also suggesting the targeting of the gene may have a potential as an antibacterial strategy, especially against drug-resistant strains[64]. Finally, the MIC of HP1043-targeting PNAs was evaluated here, allowing the verification of the antisense approach and its specificity. A promising PNA (6124) obtained the most marked specificity, as match-mismatch MIC differences were clearly observed, and antimicrobial activity on *H. pylori*, with MIC reaching 4 μM. The antisense effect was additionally confirmed by examining HP1043 protein levels in post-treatment (Figure 18). However, no significant morphological difference was observed for the match and the mismatch, with minor variations compared to the non-treated sample (Figure 19). Hence, we excluded a correlation with the lower protein expression based on current data.

The study presents a thorough investigation of the potential therapeutic use of antisense PNAs in *H. pylori* targeting HP1043, highlighting the significance of the TR in the cell, its efficiency in being taken up, and BPP-PNA's ability to silence genes. Overall, these findings collectively provide valuable insights into the development of innovative antimicrobial strategies targeting HP1043. As described in this work, the search for effective antimicrobial agents remains an ongoing and dynamic process, and our findings can lay the base for further research and development in refining antimicrobial approaches and ultimately enhancing treatment success against *H. pylori* infections.

6. REFERENCES

1. Hooi, J. K. Y. *et al.* Global Prevalence of Helicobacter pylori Infection: Systematic Review and Meta-Analysis. *Gastroenterology* **153**, 420–429 (2017).
2. Du, M.-Q. & Isaccson, P. G. Gastric MALT lymphoma: from aetiology to treatment. *Lancet Oncol.* **3**, 97–104 (2002).
3. Chmiela, M. & Kupcinskas, J. Review: Pathogenesis of *Helicobacter pylori* infection. *Helicobacter* **24**, (2019).
4. Tacconelli, E. *et al.* Discovery, research, and development of new antibiotics: the WHO priority list of antibiotic-resistant bacteria and tuberculosis. *Lancet Infect. Dis.* **18**, 318–327 (2018).
5. Leja, M., Axon, A. & Brenner, H. Epidemiology of *Helicobacter pylori* infection. *Helicobacter* **21**, 3–7 (2016).
6. Niehus, E. *et al.* Genome-wide analysis of transcriptional hierarchy and feedback regulation in the flagellar system of Helicobacter pylori: Flagellar regulation network in H. pylori. *Mol. Microbiol.* **52**, 947–961 (2004).
7. Ansari, S. & Yamaoka, Y. Helicobacter pylori Virulence Factors Exploiting Gastric Colonization and its Pathogenicity. *Toxins* **11**, 677 (2019).
8. *Helicobacter pylori in Human Diseases: Advances in Microbiology, Infectious Diseases and Public Health Volume 11*. vol. 1149 (Springer International Publishing, 2019).
9. Schneider, S. *et al.* Complex Cellular Responses of Helicobacter pylori-Colonized Gastric Adenocarcinoma Cells. *Infect. Immun.* **79**, 2362–2371 (2011).
10. Vannini, A., Roncarati, D. & Danielli, A. The cag-pathogenicity island encoded CncR1 sRNA oppositely modulates Helicobacter pylori motility and adhesion to host cells. *Cell. Mol. Life Sci.* **73**, 3151–3168 (2016).
11. Fallone, C. A. *et al.* The Toronto Consensus for the Treatment of Helicobacter pylori Infection in Adults. *Gastroenterology* **151**, 51-69.e14 (2016).
12. Boyanova, L., Evstatiev, I., Yordanov, D., Markovska, R. & Mitov, I. Three unsuccessful treatments of Helicobacter pylori infection by a highly virulent strain with quadruple antibiotic resistance. *Folia Microbiol. (Praha)* **61**, 307–310 (2016).
13. Perna, F. *et al.* Levofloxacin-based triple therapy for Helicobacter pylori re-treatment: Role of bacterial resistance. *Dig. Liver Dis.* **39**, 1001–1005 (2007).
14. González, A., Casado, J. & Lanas, Á. Fighting the Antibiotic Crisis: Flavonoids as Promising Antibacterial Drugs Against Helicobacter pylori Infection. *Front. Cell. Infect. Microbiol.* **11**, 709749 (2021).
15. Svennerholm, A.-M. & Lundgren, A. Progress in vaccine development against *Helicobacter pylori*. *FEMS Immunol. Med. Microbiol.* **50**, 146–156 (2007).
16. Visweswariah, S. S. & Busby, S. J. W. Evolution of bacterial transcription factors: how proteins take on new tasks, but do not always stop doing the old ones. *Trends Microbiol.* **23**, 463–467 (2015).
17. Baltrus, D. A. *et al.* The Complete Genome Sequence of *Helicobacter pylori* Strain G27. *J. Bacteriol.* **191**, 447–448 (2009).
18. Tomb, J.-F. *et al.* The complete genome sequence of the gastric pathogen Helicobacter pylori. *Nature* **388**, 539–547 (1997).
19. Alm, R. A. *et al.* Genomic-sequence comparison of two unrelated isolates of the human gastric pathogen Helicobacter pylori. *Nature* **397**, 176–180 (1999).

20. De Reuse, H. & Bereswill, S. Ten years after the first *Helicobacter pylori* genome: comparative and functional genomics provide new insights in the variability and adaptability of a persistent pathogen: Table 1. *FEMS Immunol. Med. Microbiol.* **50**, 165–176 (2007).
21. De La Cruz, M. A. *et al.* Gene Expression Profiling of Transcription Factors of Helicobacter pylori under Different Environmental Conditions. *Front. Microbiol.* **8**, (2017).
22. Scarlato, V., Delany, I., Spohn, G. & Beier, D. Regulation of transcription in Helicobacter pylori: simple systems or complex circuits? *Int. J. Med. Microbiol.* **291**, 107–117 (2001).
23. Douillard, F. P. *et al.* Posttranscriptional Regulation of Flagellin Synthesis in *Helicobacter pylori* by the RpoN Chaperone HP0958. *J. Bacteriol.* **190**, 7975–7984 (2008).
24. Sharma, C. M. *et al.* The primary transcriptome of the major human pathogen Helicobacter pylori. *Nature* **464**, 250–255 (2010).
25. Nguyen, T. *et al.* The Prevalence of *Helicobacter pylori* Remains High in African American and Hispanic Veterans. *Helicobacter* **20**, 305–315 (2015).
26. Vannini, A., Roncarati, D., D'Agostino, F., Antoniciello, F. & Scarlato, V. Insights into the Orchestration of Gene Transcription Regulators in Helicobacter pylori. *Int. J. Mol. Sci.* **23**, 13688 (2022).
27. Pelliciari, S., Vannini, A., Roncarati, D. & Danielli, A. The allosteric behavior of Fur mediates oxidative stress signal transduction in Helicobacter pylori. *Front. Microbiol.* **6**, (2015).
28. Pflock, M. *et al.* The Orphan Response Regulator HP1021 of *Helicobacter pylori* Regulates Transcription of a Gene Cluster Presumably Involved in Acetone Metabolism. *J. Bacteriol.* **189**, 2339–2349 (2007).
29. Waidner, B., Melchers, K., Stähler, F. N., Kist, M. & Bereswill, S. The *Helicobacter pylori* CrdRS Two-Component Regulation System (HP1364/HP1365) Is Required for Copper-Mediated Induction of the Copper Resistance Determinant CrdA. *J. Bacteriol.* **187**, 4683–4688 (2005).
30. Schär, J., Sickmann, A. & Beier, D. Phosphorylation-Independent Activity of Atypical Response Regulators of *Helicobacter pylori*. *J. Bacteriol.* **187**, 3100–3109 (2005).
31. Noszka, M. *et al.* Profiling of the Helicobacter pylori redox switch HP1021 regulon using a multi-omics approach. *Nat. Commun.* **14**, 6715 (2023).
32. Szczepanowski, P. *et al.* HP1021 is a redox switch protein identified in *Helicobacter pylori*. *Nucleic Acids Res.* **49**, 6863–6879 (2021).
33. Donczew, R. *et al.* The atypical response regulator HP1021 controls formation of the *H elicobacter pylori* replication initiation complex: HP1021 affects orisome formation in *H. pylori*. *Mol. Microbiol.* **95**, 297–312 (2015).
34. Pelliciari, S. *et al.* Insight into the essential role of the Helicobacter pylori HP1043 orphan response regulator: genome-wide identification and characterization of the DNA-binding sites. *Sci. Rep.* **7**, 41063 (2017).
35. Zannoni, A. *et al.* Definition of the Binding Architecture to a Target Promoter of HP1043, the Essential Master Regulator of Helicobacter pylori. *Int. J. Mol. Sci.* **22**, 7848 (2021).
36. Danielli, A. & Scarlato, V. Regulatory circuits in *Helicobacter pylori* : network motifs and regulators involved in metal-dependent responses. *FEMS Microbiol. Rev.* **34**, 738–752 (2010).
37. Roncarati, D. & Scarlato, V. The Interplay between Two Transcriptional Repressors and Chaperones Orchestrates Helicobacter pylori Heat-Shock Response. *Int. J. Mol. Sci.* **19**, 1702 (2018).
38. Bischler, T., Tan, H. S., Nieselt, K. & Sharma, C. M. Differential RNA-seq (dRNA-seq) for annotation of transcriptional start sites and small RNAs in Helicobacter pylori. *Methods* **86**, 89–101 (2015).
39. Pernitzsch, S. R. & Sharma, C. M. Transcriptome Complexity and Riboregulation in the Human Pathogen Helicobacter pylori. *Front. Cell. Infect. Microbiol.* **2**, (2012).

40. Josenhans, C., Beier, D., Linz, B., Meyer, T. F. & Suerbaum, S. Pathogenomics of Helicobacter. *Int. J. Med. Microbiol.* **297**, 589–600 (2007).
41. Haugen, S. P., Ross, W. & Gourse, R. L. Advances in bacterial promoter recognition and its control by factors that do not bind DNA. *Nat. Rev. Microbiol.* **6**, 507–519 (2008).
42. Pflock, M., Kennard, S., Delany, I., Scarlato, V. & Beier, D. Acid-Induced Activation of the Urease Promoters Is Mediated Directly by the ArsRS Two-Component System of *Helicobacter pylori*. *Infect. Immun.* **73**, 6437–6445 (2005).
43. Müller, S., Pflock, M., Schär, J., Kennard, S. & Beier, D. Regulation of expression of atypical orphan response regulators of Helicobacter pylori. *Microbiol. Res.* **162**, 1–14 (2007).
44. Hong, E. *et al.* Structure of an Atypical Orphan Response Regulator Protein Supports a New Phosphorylation-independent Regulatory Mechanism. *J. Biol. Chem.* **282**, 20667–20675 (2007).
45. Blanco, A. G., Sola, M., Gomis-Rüth, F. X. & Coll, M. Tandem DNA Recognition by PhoB, a Two-Component Signal Transduction Transcriptional Activator. *Structure* **10**, 701–713 (2002).
46. Delany, I., Spohn, G., Rappuoli, R. & Scarlato, V. The Fur repressor controls transcription of iron-activated and -repressed genes in Helicobacter pylori: Iron regulation in H. pylori. *Mol. Microbiol.* **42**, 1297–1309 (2002).
47. Jeong, K.-W. *et al.* Backbone dynamics of an atypical orphan response regulator protein, Helicobacter pylori 1043. *Mol. Cells* **35**, 158–165 (2013).
48. Hong, E. *et al.* Letter to the Editor: Backbone ^{1}H, ^{13}C and ^{15}N resonance assignments of the response regulator HP1043 from Helicobactor pylori. *J. Biomol. NMR* **28**, 85–86 (2004).
49. Pelliciari, S. *Biochemical and functional characterization of the HP1043 orphan response regulator of the human pathogen Helicobacter pylori*. (2018).
50. Olekhnovich, I. N., Vitko, S., Valliere, M. & Hoffman, P. S. Response to Metronidazole and Oxidative Stress Is Mediated through Homeostatic Regulator HsrA (HP1043) in Helicobacter pylori. *J. Bacteriol.* **196**, 729–739 (2014).
51. Azevedo, N. F. *et al.* Coccoid Form of *Helicobacter pylori* as a Morphological Manifestation of Cell Adaptation to the Environment. *Appl. Environ. Microbiol.* **73**, 3423–3427 (2007).
52. Browning, D. F. & Busby, S. J. W. Local and global regulation of transcription initiation in bacteria. *Nat. Rev. Microbiol.* **14**, 638–650 (2016).
53. Olekhnovich, I. N. *et al.* Mutations to Essential Orphan Response Regulator HP1043 of Helicobacter pylori Result in Growth-Stage Regulatory Defects. *Infect. Immun.* **81**, 1439–1449 (2013).
54. Delany, I., Spohn, G., Rappuoli, R. & Scarlato, V. Growth Phase-Dependent Regulation of Target Gene Promoters for Binding of the Essential Orphan Response Regulator HP1043 of *Helicobacter pylori*. *J. Bacteriol.* **184**, 4800–4810 (2002).
55. González, A. *et al.* Identifying potential novel drugs against Helicobacter pylori by targeting the essential response regulator HsrA. *Sci. Rep.* **9**, 11294 (2019).
56. Roncarati, D., Scarlato, V. & Vannini, A. Targeting of Regulators as a Promising Approach in the Search for Novel Antimicrobial Agents. *Microorganisms* **10**, 185 (2022).
57. Pernitzsch, S. R. *et al.* Small RNA mediated gradual control of lipopolysaccharide biosynthesis affects antibiotic resistance in Helicobacter pylori. *Nat. Commun.* **12**, 4433 (2021).
58. Lee, Z.-W. *et al.* Small-molecule inhibitor of HlyU attenuates virulence of Vibrio species. *Sci. Rep.* **9**, 4346 (2019).
59. Good, L. & Nielsen, P. E. Antisense inhibition of gene expression in bacteria by PNA targeted to mRNA. *Nat. Biotechnol.* **16**, 355–358 (1998).
60. Good, L. & Nielsen, P. E. Inhibition of translation and bacterial growth by peptide nucleic acid targeted to ribosomal RNA. *Proc. Natl. Acad. Sci.* **95**, 2073–2076 (1998).

61. Goltermann, L., Yavari, N., Zhang, M., Ghosal, A. & Nielsen, P. E. PNA Length Restriction of Antibacterial Activity of Peptide-PNA Conjugates in Escherichia coli Through Effects of the Inner Membrane. *Front. Microbiol.* **10**, 1032 (2019).
62. Pifer, R. & Greenberg, D. E. Antisense antibacterial compounds. *Transl. Res.* **223**, 89–106 (2020).
63. Dryselius, R., Aswasti, S. K., Rajarao, G. K., Nielsen, P. E. & Good, L. The Translation Start Codon Region Is Sensitive to Antisense PNA Inhibition in *Escherichia coli*. *Oligonucleotides* **13**, 427–433 (2003).
64. Nejad, A. J., Shahrokhi, N. & Nielsen, P. E. Targeting of the Essential acpP, ftsZ, and rne Genes in Carbapenem-Resistant Acinetobacter baumannii by Antisense PNA Precision Antibacterials. *Biomedicines* **9**, 429 (2021).
65. Good, L., Awasthi, S. K., Dryselius, R., Larsson, O. & Nielsen, P. E. Bactericidal antisense effects of peptide–PNA conjugates. *Nat. Biotechnol.* **19**, 360–364 (2001).
66. Yavari, N., Goltermann, L. & Nielsen, P. E. Uptake, Stability, and Activity of Antisense Anti-*acpP* PNA-Peptide Conjugates in *Escherichia coli* and the Role of SbmA. *ACS Chem. Biol.* **16**, 471–479 (2021).
67. Popella, L. *et al.* Comprehensive analysis of PNA-based antisense antibiotics targeting various essential genes in uropathogenic *Escherichia coli*. *Nucleic Acids Res.* **50**, 6435–6452 (2022).
68. Iubatti, M. *et al.* Antisense Peptide Nucleic Acid–Diaminobutanoic Acid Dendron Conjugates with SbmA-Independent Antimicrobial Activity against Gram-Negative Bacteria. *ACS Infect. Dis.* **8**, 1098–1106 (2022).
69. Goltermann, L. *et al.* Effects of LPS Composition in Escherichia coli on Antibacterial Activity and Bacterial Uptake of Antisense Peptide-PNA Conjugates. *Front. Microbiol.* **13**, 877377 (2022).
70. Frimodt-Møller, J. *et al.* Activating the Cpx response induces tolerance to antisense PNA delivered by an arginine-rich peptide in Escherichia coli. *Mol. Ther. - Nucleic Acids* **25**, 444–454 (2021).
71. Pushpakom, S. *et al.* Drug repurposing: progress, challenges and recommendations. *Nat. Rev. Drug Discov.* **18**, 41–58 (2019).
72. Rouhana, S., Virsolvy, A., Fares, N., Richard, S. & Thireau, J. Ranolazine: An Old Drug with Emerging Potential; Lessons from Pre-Clinical and Clinical Investigations for Possible Repositioning. *Pharmaceuticals* **15**, 31 (2021).
73. González, A. *et al.* 1,4-Dihydropyridine as a Promising Scaffold for Novel Antimicrobials Against Helicobacter pylori. *Front. Microbiol.* **13**, 874709 (2022).
74. Antoniciello, F. *et al.* Targeting the Essential Transcription Factor HP1043 of Helicobacter pylori: A Drug Repositioning Study. *Front. Mol. Biosci.* **9**, 887564 (2022).
75. Panche, A. N., Diwan, A. D. & Chandra, S. R. Flavonoids: an overview. *J. Nutr. Sci.* **5**, e47 (2016).
76. Havsteen, B. H. The biochemistry and medical significance of the flavonoids. *Pharmacol. Ther.* **96**, 67–202 (2002).
77. Qiao, N. *et al.* Pharmaceutical cocrystals: An overview. *Int. J. Pharm.* **419**, 1–11 (2011).
78. Duggirala, N. K., Perry, M. L., Almarsson, Ö. & Zaworotko, M. J. Pharmaceutical cocrystals: along the path to improved medicines. *Chem. Commun.* **52**, 640–655 (2016).
79. Fiore, C. *et al.* Inhibition of the Antibiotic Activity of Cephalosporines by Co-Crystallization with Thymol. *Cryst. Growth Des.* **22**, 1467–1475 (2022).
80. Shemchuk, O. *et al.* Natural Antimicrobials Meet a Synthetic Antibiotic: Carvacrol/Thymol and Ciprofloxacin Cocrystals as a Promising Solid-State Route to Activity Enhancement. *Cryst. Growth Des.* **20**, 6796–6803 (2020).

81. McColl, K. E. L. *Helicobacter pylori* Infection. *N. Engl. J. Med.* **362**, 1597–1604 (2010).
82. Yang, H., Guan, L. & Hu, B. Detection and Treatment of Helicobacter pylori: Problems and Advances. *Gastroenterol. Res. Pract.* **2022**, 1–10 (2022).
83. Anand, U. *et al.* A review on antimicrobial botanicals, phytochemicals and natural resistance modifying agents from Apocynaceae family: Possible therapeutic approaches against multidrug resistance in pathogenic microorganisms. *Drug Resist. Updat.* **51**, 100695 (2020).
84. Salomon-Ferrer, R., Case, D. A. & Walker, R. C. An overview of the Amber biomolecular simulation package. *WIREs Comput. Mol. Sci.* **3**, 198–210 (2013).
85. Maier, J. A. *et al.* ff14SB: Improving the Accuracy of Protein Side Chain and Backbone Parameters from ff99SB. *J. Chem. Theory Comput.* **11**, 3696–3713 (2015).
86. Cheatham, T. E. & Case, D. A. Twenty-five years of nucleic acid simulations. *Biopolymers* **99**, 969–977 (2013).
87. Miller, B. R. *et al. MMPBSA.py* : An Efficient Program for End-State Free Energy Calculations. *J. Chem. Theory Comput.* **8**, 3314–3321 (2012).
88. Onufriev, A., Bashford, D. & Case, D. A. Exploring protein native states and large-scale conformational changes with a modified generalized born model. *Proteins Struct. Funct. Bioinforma.* **55**, 383–394 (2004).
89. Sambrook, J. & Green, M. R. *Molecular cloning: a laboratory manual.* (Cold Spring Harbor Laboratory Press - Cold Spring Harbor, 2012).
90. Chevalier, C., Thiberge, J.-M., Ferrero, R. L. & Labigne, A. Essential role of Helicobacter pylori gamma-glutamyltranspeptidase for the colonization of the gastric mucosa of mice. *Mol. Microbiol.* **31**, 1359–1372 (1999).
91. Livak, K. J. & Schmittgen, T. D. Analysis of Relative Gene Expression Data Using Real-Time Quantitative PCR and the 2−ΔΔCT Method. *Methods* **25**, 402–408 (2001).
92. Goltermann, L. & Nielsen, P. E. PNA Antisense Targeting in Bacteria: Determination of Antibacterial Activity (MIC) of PNA-Peptide Conjugates. in *Peptide Nucleic Acids* (ed. Nielsen, P. E.) vol. 2105 231–239 (Springer US, 2020).
93. Xiang, Z. *et al.* Analysis of expression of CagA and VacA virulence factors in 43 strains of Helicobacter pylori reveals that clinical isolates can be divided into two major types and that CagA is not necessary for expression of the vacuolating cytotoxin. *Infect. Immun.* **63**, 94–98 (1995).
94. Hanahan, D. Studies on transformation of Escherichia coli with plasmids. *J. Mol. Biol.* **166**, 557–580 (1983).
95. Vannini, A., Roncarati, D., Spinsanti, M., Scarlato, V. & Danielli, A. In Depth Analysis of the Helicobacter pylori cag Pathogenicity Island Transcriptional Responses. *PLoS ONE* **9**, e98416 (2014).
96. Cook, T. B. *et al.* Genetic tools for reliable gene expression and recombineering in *Pseudomonas putida*. *J. Ind. Microbiol. Biotechnol.* **45**, 517–527 (2018).
97. Pepe, S. *et al.* The Helicobacter pylori Heat-Shock Repressor HspR: Definition of Its Direct Regulon and Characterization of the Cooperative DNA-Binding Mechanism on Its Own Promoter. *Front. Microbiol.* **9**, 1887 (2018).
98. Vannini, A. *et al.* A Convenient and Robust *In Vivo* Reporter System To Monitor Gene Expression in the Human Pathogen Helicobacter pylori. *Appl. Environ. Microbiol.* **78**, 6524–6533 (2012).
99. Gisbert, J. P. *et al.* Second-line Therapy With Levofloxacin After Failure of Treatment to Eradicate Helicobacter pylori Infection: Time Trends in a Spanish Multicenter Study of 1000 Patients. *J. Clin. Gastroenterol.* **47**, 130–135 (2013).

100. Di Caro, S. *et al.* Second-line levofloxacin-based triple schemes for Helicobacter pylori eradication. *Dig. Liver Dis.* **41**, 480–485 (2009).
101. Dresner, D. *et al.* Efficacy of Ciprofloxacin in the Eradication of Helicobacter pylori: *South. Med. J.* **89**, 775–778 (1996).
102. Tshibangu-Kabamba, E. & Yamaoka, Y. Helicobacter pylori infection and antibiotic resistance — from biology to clinical implications. *Nat. Rev. Gastroenterol. Hepatol.* **18**, 613–629 (2021).
103. Bai, H. *et al.* Antisense inhibition of gene expression and growth in gram-negative bacteria by cell-penetrating peptide conjugates of peptide nucleic acids targeted to rpoD gene. *Biomaterials* **33**, 659–667 (2012).
104. Ghosal, A. & Nielsen, P. E. Potent Antibacterial Antisense Peptide–Peptide Nucleic Acid Conjugates Against *Pseudomonas aeruginosa*. *Nucleic Acid Ther.* **22**, 323–334 (2012).